20mip

NASA CR-132,431
UCLA-ENG-7406
FEBRUARY 1974

AEROELASTIC STABILITY OF COUPLED FLAP-LAG MOTION OF HINGELESS HELICOPTER BLADES AT ARBITRARY ADVANCE RATIOS

P. FRIEDMANN
L.J. SILVERTHORN

UCLA • SCHOOL OF ENGINEERING AND APPLIED SCIENCE

1. Report No.	2. Government Accession No.	3. Recipient's Catalog No.
NASA CR-132431		

4. Title and Subtitle	5. Report Date
AEROELASTIC STABILITY OF COUPLED FLAP-LAG MOTION OF HINGELESS HELICOPTER BLADES AT ARBITRARY ADVANCE RATIOS	February, 1974
	6. Performing Organization Code

7. Author(s)	8. Performing Organization Report No.
PERETZ FRIEDMANN AND LOUIS J. SILVERTHORN	UCLA – Eng – 7406

9. Performing Organization Name and Address	10. Work Unit No.
Mechanics and Structures Dept. School of Engineering and Applied Science University of California Los Angeles, Calif. 90024	
	11. Contract or Grant No.
	NGR 05-007-414
	13. Type of Report and Period Covered

12. Sponsoring Agency Name and Address	
Langley Directorate, U.S. Army Air Mobility Research and Development Laboratory Langley Research Center, Hampton, Va. 23665	14. Sponsoring Agency Code

15. Supplementary Notes

Technical Monitor: Dr. C.E. Hammond
Langley Directorate, U.S. Army Air Mobility Research and Development Laboratory
Langley Research Center, Hampton, Ba. 23665

16. Abstract

Equations for large amplitude coupled flap-lag motion of a hingeless elastic helicopter blade in forward flight are derived. Only a torsionally rigid blade excited by quasi-steady aerodynamic loads is considered. The effects of reversed flow together with some new terms due to radial flow are included. Using Galerkin's method the spatial dependence is eliminated and the equations are linearized about a suitable equilibrium position.

The resulting system of homogeneous periodic equations is solved using multivariable Floquet-Liapunov theory, and the transition matrix at the end of the period is evaluated by two separate methods. Computational efficiency of the two numerical methods is compared. Results illustrating the effects of forward flight and various important blade parameters on the stability boundaries are presented.

17. Key Words (Suggested by Author(s)) (STAR category underlined)	18. Distribution Statement
Helicopter Aeroelasticity Rotor Blade Dynamics VTOL Vibration Structural Dynamics Aeroelasticity Dynamic Stability	Unclassified, Unlimited

19. Security Classif. (of this report)	20. Security Classif. (of this page)	21. No. of Pages	22. Price*
Unclassified	Unclassified	89	

AEROELASTIC STABILITY OF COUPLED FLAP-LAG MOTION OF

HINGELESS HELICOPTER BLADES AT ARBITRARY

ADVANCE RATIOS

Peretz Friedmann
Louis J. Silverthorn

Mechanics and Structures Department
School of Engineering and Applied Science
University of California
Los Angeles, California   90024

FOREWORD

This research was conducted at the Mechanics and Structures Department, School of Engineering and Applied Science, University of California, Los Angeles under NASA Grant NGR 05-007-414 monitored by Dr. C.E. Hammond, Langley Directorate, U.S. Army Air Mobility R & D Laboratory, NASA/Langley Research Center, Hampton, Virginia.

The authors wish to express their appreciation to Dr. C.E. Hammond for his useful comments and suggestions.

The authors are indebted to Dr. E.R. Wood for his helpful advice in the course of this study.

PRECEDING PAGE BLANK NOT FILMED

CONTENTS

LIST OF FIGURES

LIST OF SYMBOLS

a	Two dimensional lift-curve slope
$\bar{A}$	Tip loss coefficient
$\underset{\sim}{A}$	Periodic matrix with elements A_{ij} defined in Appendix C
A_{Fi}, A_{Li}	Generalized aerodynamic force for i^{th} flap and lag mode respectively
$\bar{A}_{Fi}$, $\bar{A}_{Li}$	Generalized aerodynamic force in reverse and mixed flow regions for i^{th} flap and lag mode respectively
b	Semi-chord nondimensionalized with respect to R
$\bar{B}$	Tip loss factor
$\bar{B}^i$	Generalized masses defined in Appendix B
C_T	Thrust coefficient
$\underset{\sim}{C}$	Constant matrix
$\underset{\sim}{C}_k$	Constant matrix approximation over k^{th} interval of $\underset{\sim}{A}(\psi)$
C_{Do}	Profile drag coefficient
$C(k)$	Theodorsen's lift deficiency function
e_1	Defined in Fig. 1
e_A	Distance between area centroid of tensile member and elastic axis
E_{c1}, E_{c2}, $\bar{E}^s_{ik}$ $\bar{E}^s_{im}$, $\bar{E}^{cs}_{im}$, $\bar{E}^{cs}_{ik}$	Terms associated with elastic coupling effect defined in Appendix E
$(EI)_y$	Bending stiffness in flap direction
$(EI)_z$	Bending stiffness in lead-lag direction
$\underset{\sim}{f}$	Periodic forcing vector defined in Appendix C
F^i	Flap coefficients defined in Appendix B

g_k — Generalized coordinate, k^{th} normal flapping mode

g_k^o — Static value of g_k in hover

Δg_k — Perturbation in g_k about g_k^o

g_{sF}, g_{sL} — Viscous structural damping in flap and lag respectively

$\underset{\sim}{H}(k)$ — Growth matrix

h_m — Generalized coordinate, m^{th} normal inplane mode

h_m^o — Static value of h_m in hover

Δh_m — Perturbation in h_m about h_m^o

i — $\sqrt{-1}$

$\underset{\sim}{i}$, $\underset{\sim}{j}$, $\underset{\sim}{k}$ — Unit vectors in the x , y and z directions (Fig. 1)

I_b — Mass moment of inertia of elastic part of the blade about its root, defined in Appendix B

$\underset{\sim}{I}$ — Unit matrix

J — Integer used in Eq. (3.27)

ℓ — Length of blade capable of elastic deformation

L^i — Lag coefficients defined in Appendix B

L_y, L_z — Aerodynamic load per unit length in the y and z directions respectively

m — Mass of blade per unit length

M, N — Number of modes in flap and lag respectively

$\bar{M}_{Fi}$, $\bar{M}_{Li}$ — Generalized mass for the ith flap and lag mode respectively, defined in Appendiz B

$\left(\bar{M}_\eta\right)_{ik\ell}$, $\left(\bar{M}_\gamma\right)_{imr}$ — Defined in Appendix B

n_b — Number of blades

P_x, P_y, P_z — Resultant total loading per unit length in the x, y and z directions respectively

$\underset{\sim}{P}(\psi)$ — Periodic matrix

$\bar{P}_{1km}$ — Defined in Appendix B

$\underset{\sim}{Q}$ — Constant matrix

R — Blade radius

$\underset{\sim}{R}$ — Constant matrix used in Floquet–Liapunov theorem

$\underset{\sim}{S}$ — Matrix associated with the calculation of the linear static equilibrium position of the blade

T — Common nondimensional period, also used for tension in the blade

u, v, w — x, y and z displacements of a point on the elastic axis of the blade

U — Airstream velocity with respect to the blade at station x

U_p — Component of U perpendicular to x-y plane (hub plane), positive down

U_T — Component of U in the x-y plane tangent to a circle of radius x

$U(\psi)$ — Heaviside unit step function

v_e — Elastic part of the displacement of a point on the elastic axis of the blade in the $\underset{\sim}{j}$ direction, Fig. 1

v_{e_o} — Static equilibrium value of v_e

V — Velocity of forward flight of the whole rotor

w_e — Elastic part of the displacement of a point on the elastic axis of the blade approximately in the $\underset{\sim}{k}$ direction, Fig. 1

w_{e_o} — Static equilibrium value of w_e

x, y, z — Rotating orthogonal coordinate system, Fig. 1

$x_o = x - e_1$ — Running spanwise coordinate for part of the blade free to deflect elastically

$\underset{\sim}{y}$ — State variable column matrix

xi

Greek

α	Angle of reversed flow region (Fig. 2)
α_R	Angle of attack of the whole rotor
β_D	Droop, built-in angle of the undeformed position of the blade measured from the feathering axis (fig. 1)
β_P	Preconing inclination of the feathering axis with respect to the hub plane measured in a vertical plane
γ	Lock number $\gamma = \left(2\rho_A \dfrac{bR^5 a}{I_b} \right)$, based on normal flow
γ_m	m^{th} inplane bending mode
ε_D	Symbolic quantity having the same order of magnitude of the displacements v and w
ζ_k	Real part of the kth characteristic exponent
η_k	k^{th} flapwise bending mode
η_{SFi}, η_{SLi}	Viscous structural damping coefficients defined in Appendix B
θ	Collective pitch angle measured from the x-y plane, in radians
θ_c	Critical value of collective pitch at which the linearized coupled flap-lag system becomes unstable in hover
λ	Inflow ratio, induced velocity over disk, positive down, nondimensionalized with respect to ΩR
$\underset{\sim}{\lambda}$	Diagonal matrix containing eigenvalues λ_k of $\underset{\sim}{R}$
$\underset{\sim}{\Lambda}$	Diagonal matrix containing eigenvalues Λ_k of $\underset{\sim}{\Phi}(T,0)$
μ	Advance ratio
μ_c	Critical value of advance ratio at which flap-lag system becomes unstable
ρ_A	Density of air
σ	Blade solidity ratio $= \dfrac{2bn_b}{R\pi}$

$\underset{\sim}{\Phi}(\psi,\psi_o)$	State transition matrix at ψ for initial conditions given at ψ_o
ψ	Azimuth angle of blade ($\psi = \Omega t$) measured from straight aft position
ω_c	Flutter frequency in hover
ω_k	Imaginary part of kth characteristic exponent
$\omega_{Fi},\ \omega_{Li}$	Natural frequency of the ith rotating flap or lag mode respectively
$\bar{\omega}_{F1N},\ \bar{\omega}_{L1N}$	First nonrotating natural frequency in flap and lag, respectively nondimensionalized w.r.t. Ω.
Ω	Speed of rotation

Special Symbols

$\bar{(\ )}$	Nondimensionalized quantity, lengths associated with elastic properties nondimensionalized with respect to ℓ, all others with respect to R; frequencies with respect to Ω; mass properties with respect to I_b
$(\ )'$	Differentiation with respect to $\bar{x}_o$
$\overset{*}{(\ )}$	Differentiation with respect to ψ
$(\ )_R,\ (\ )_I$	Subscripts denoting real and imaginary parts of the appropriate quantity
$\underset{\sim}{(\ )}$	Vector or matrix
$\underset{\sim}{(\ )}^{-1}$	Inverse of a matrix

SECTION 1

INTRODUCTION

The dynamics of a helicopter blade in forward flight are usually
described by a system of differential equations with periodic coefficients.
A growing acceptance of hingeless helicopter blades for conventional
helicopters flying at relatively high forward flight speeds has intensified
the need for fundamental research on the aeroelastic stability of such
systems.

Studies dealing with the effect of forward flight (or periodic
coefficients) have been primarily devoted to the study of flapping insta-
bility at high advance ratios (Refs. 1 through 8). A limited number of
studies dealing with the effect of periodic coefficients on coupled flap-
lag (Refs. 9 and 10) or coupled flap-lag-pitch (Ref. 11) motion were also
conducted. The case of coupled flap-lag motion has been, somewhat incon-
clusively, investigated by Hall (Ref. 10) using multivariable Floquet
theory. The same problem was also considered by Friedmann and Tong (Ref. 9)
but the treatment was limited to low advance ratios ($\mu < 0.3$). Coupled,
linearized, flap-lag-torsion motion has been investigated by Crimi
(Ref. 11) using a modified Hill method. In both cases (Refs. 10 and 11)
only a limited number of numerical results were obtained and the physical
mechanism of the aeroelastic instabilities has not been clearly identified.
In particular, the degree of freedom which is responsible for the instability
was not identified and the results for forward flight were not compared
with those for hover.

1

Recent investigation of the aeroelastic stability of hingeless blades in hover (Ref. 12) indicated that the aeroelastic stability boundaries are quite sensitive to the number of degrees of freedom employed in the analysis. Therefore it is important to determine how the flapping behavior of a blade at high advance ratios is modified by the inclusion of the lag degree of freedom. This important problem, which has not received adequate treatment before, is one of the main topics of the present study.

The mathematical methods used in previous studies dealing with the effects of forward flight were:

(a) The rectangular ripple method (Ref. 1)

(b) Analog computer simulation (Refs. 3 and 4)

(c) Various variations of Hill's method (Refs. 2 and 11)

(d) Multivariable Floquet-Liapunov theory (Refs. 6, 7 and 10)

(e) Perturbation method in multiple time scales (Refs. 8 and 9)

The mathematical method employed in the present study is the Floquet-Liapunov theorem, and the transition matrix is evaluated by two separate methods:

1. Direct numerical integration using a fourth order Runge-Kutta method

2. A new and computationally efficient method developed by Hsu (Refs. 23 through 25) which is a multivariable extension of the rectangular ripple method.

It is also shown that careful use of these methods enables one to circumvent problems associated with identifying the results encountered in previous studies (Ref. 10).

In addition, a new and convenient approximation for the reversed flow region is developed. This approximation is believed to be adequate for

2

most blade stability analyses. Finally, the effects of various important parameters such as collective pitch setting, structural damping, droop and precone on the stability associated with forward flight are investigated.

SECTION 2

THE EQUATIONS OF MOTION

2.1 Basic Assumptions

The geometry of the problem is shown in Fig. 1. The following basic assumptions were used in deriving the equations of motion: (a) The blade is cantilevered at the rotor hub. It can have an angle of droop β_D at the root. In addition, the feathering axis can be preconed by an angle β_P. The angles β_D and β_P are small. (b) The blade is torsionally rigid and can bend in two directions normal to the elastic axis. (c) The deflections of the blade are moderately small so that terms of $O(\varepsilon_D{}^2)$ can be neglected compared to one. (d) Moderately large deflections have only a small effect on the tension due to elastic effects since one of its ends is free, therefore a linear treatment of the elastic restoring forces is adequate. (e) A two-dimensional aerodynamic strip theory is used with $C(k) = 1$ and apparent mass effects are neglected. (f) Stall and compressibility effects are neglected. (g) Reversed flow is included using an approximate model for reversed flow described in Appendix D. (h) A single blade analysis is performed, where the blade is attached to an aircraft with infinite mass.

In deriving the equations of motion, an x, y, x coordinate system (Fig. 1) rotating with the shaft of the helicopter and attached to the blade is used.

2.2 Derivation of the Equations of Motion

The equations of dynamic equilibrium of a blade undergoing only bending in flap and lag can be taken from Friedmann (Ref. 13):

5

$$\frac{\partial^2}{\partial x_o^2} \left\{ \left[(EI)_y \cos^2 \Theta + (EI)_z \sin^2 \Theta \right] \frac{\partial^2 w_e}{\partial x_o^2} \right.$$

$$+ \left[(EI)_z - (EI)_y \right] \sin \Theta \cos \Theta \frac{\partial^2 v_e}{\partial x_o^2}$$

$$\left. - Te_A \sin \Theta \right\} - \frac{\partial}{\partial x_o} \left[T(x_o) \frac{\partial w}{\partial x_o} \right] = P_z \qquad (2.1)$$

$$\frac{\partial^2}{\partial x_o^2} \left\{ \left[(EI)_z - (EI)_y \right] \sin \Theta \cos \Theta \frac{\partial^2 w_e}{\partial x_o^2} + \right.$$

$$+ \left[(EI)_y \sin^2 \Theta + (EI)_z \cos^2 \Theta \right] \frac{\partial^2 v_e}{\partial x_o^2}$$

$$\left. - Te_A \cos \Theta \right\} - \frac{\partial}{\partial x_o} \left[T(x_o) \frac{\partial v}{\partial x_o} \right] = P_y$$

where P_y and P_z include the aerodynamic and inertia loads distributed along the span of the rotor blade.

Denoting the elastic coupling effect by E_{c1} and E_{c2} as defined in Appendix E, Eqs. (E.3) and (E.4), and assuming that $e_A = 0$, Eqs. (2.1) can be rewritten as

$$\frac{\partial^2}{\partial x_o^2} \left\{ \left[(EI)_y + E_{c1} \right] \frac{\partial^2 w_e}{\partial x_o^2} + E_{c2} \frac{\partial^2 v_e}{\partial x_o^2} \right\} - \frac{\partial}{\partial x_o} \left[T(x_o) \frac{\partial w}{\partial x_o} \right] = P_z \qquad (2.2)$$

$$\frac{\partial^2}{\partial x_o^2} \left\{ \left[(EI)_z - E_{c1} \right] \frac{\partial^2 v_e}{\partial x_o^2} + E_{c2} \frac{\partial^2 w_e}{\partial x_o^2} \right\} - \frac{\partial}{\partial x_o} \left[T(x_o) \frac{\partial v}{\partial x_o} \right] = P_y \qquad (2.3)$$

The loading terms in the x, y and z directions with nonlinearities up to and including second order terms in displacements can be written as (Reference 13)

$$P_x = - \frac{\partial T}{\partial x_o} = -m \, \Omega^2 \left[\overset{**}{u} - (x_o + e_1 + u) - 2\overset{*}{v} \right] \qquad (2.4)$$

$$P_y = L_y - m \, \Omega^2 \left[\overset{**}{v} - (v) + 2\overset{*}{u} \right] - g_{SL} \, \Omega \, \overset{*}{v}_e \qquad (2.5)$$

6

$$P_z = L_z - m \Omega^2 \overset{**}{w} - g_{SF} \Omega \overset{*}{w_e} \qquad (2.6)$$

where terms marked by $\nearrow$ are small[†] and have been neglected. The last terms in Eqs. (2.5 and 2.6) represent viscous type structural damping.

The boundary conditions for a cantilevered helicopter rotor blade are

$$w_e (o,t) = \frac{\partial w_e(o,t)}{\partial x_o} = \frac{\partial^2 w_e(1,t)}{\partial x_o^2} = \frac{\partial^3 w_e(1,t)}{\partial x_o^3} = 0 \qquad (2.7)$$

$$v_e (o,t) = \frac{\partial v_e(o,t)}{\partial x_o} = \frac{\partial^2 v_e(1,t)}{\partial x_o^2} = \frac{\partial^3 v_e(1,t)}{\partial x_o^3} = 0$$

The total displacements in the x,y,z directions are given by (Ref. 13)[††]

$$u = -w_e (\beta_p + \beta_d) - \frac{x_0}{2} (\beta_P + \beta_D)^2 - \frac{1}{2} \int_o^{x_o} \left[\left(\frac{\partial v_e}{\partial x_o}\right)^2 + \left(\frac{\partial w_e}{\partial x_o}\right)^2 \right] dx_1 \qquad (2.8)$$

$$v = v_e - x_o \beta_D \theta \qquad (2.9)$$

$$w = w_e + x_o (\beta_p + \beta_D) \qquad (2.10)$$

where the last term in Eq. (2.8) represents the shortening effect due to bending under the assumption of an inextensible blade.

Applying Galerkin's method on the equations of motion, the spatial variable is eliminated. This is achieved by representing the elastic part of the displacements v and w by a sum of normal modes in flap and lag respectively.

$$v_e = - \sum_m \ell \gamma_m(x_o) h_m(t) = - \ell \gamma_m h_m \qquad (2.11)$$

[†] with assumption C p.4

[††] with $\sin \theta \simeq \theta$

$$w_e = \sum_k \ell \, \eta_k \, (x_o) \, g_k \, (t) = \ell \, \eta_k \, g_k \tag{2.12}$$

where it is understood that in the present study repeated indices imply summation, unless otherwise stated. Using Eqs. (2.11) and (2.12) the displacement field can be rewritten as

$$u = -\ell \, \eta_k \, g_k \, (\beta_P + \beta_D) - \frac{\overline{x}_o \ell}{2} \, (\beta_P + \beta_D)^2$$
$$- \frac{\ell}{2} \int_0^{\overline{x}_o} \left[\left(\eta_k' \, g_k \right)^2 + \left(\gamma_m' \, h_m \right)^2 \right] \, d\overline{x}_1 \tag{2.13}$$

$$v = -\ell \, \gamma_m \, h_m - \overline{x}_o \, \ell \, \beta_D \theta \tag{2.14}$$

$$w = \ell \, \overline{x}_o \, (\beta_P + \beta_D) + \ell \, \eta_k \, g_k \tag{2.15}$$

Next Eqs. (2.13) through (2.15) are substituted into the combination of Equations (2.2) through (2.6). The resulting flap equation is multiplied by $\ell^2 \eta_i \, d\overline{x}_o$ while the lag equation is multiplied by $\ell^2 \, \gamma_i \, d\overline{x}_o$ and the equations of motion are integrated over the domain $0 < \overline{x} < 1$. In this process the integrals associated with the elastic properties of the blade are integrated between $0 < x_o < \ell$, while those associated with the aerodynamic loads are integrated between $\overline{A} < \overline{x}_o < \overline{B}$. Thus the equations in their final nondimensionalized form can be written as

$$\overline{M}_{Fi} \, \overset{**}{g}_i + 2 \, \overline{\omega}_{Fi} \, \overline{M}_{Fi} \, \eta_{SF_i} \, \overset{*}{g}_i + \overline{M}_{Fi} \, \overline{\omega}_{Fi}^2 \, g_i = \left[- \overline{E}_{ik}^s + 2\overline{P}_{ikm} \, \overset{*}{h}_m \right] g_k$$
$$- \overline{B}_i^1 (\beta_P + \beta_D) + 2(\beta_P + \beta_D)\overline{B}_{im}^3 \, \overset{*}{h}_m + \overline{E}_{im}^{cs} \, h_m + A_{Fi}$$
$$i = 1, 2, \ldots M \tag{2.16}$$

$$\overline{M}_{Li} \overset{**}{h}_i + 2\, \overline{\omega}_{Li}\, \overline{M}_{Li}\, \eta_{SLi}\, \overset{*}{h}_i + \overline{M}_{Li}\, \overline{\omega}^2_{Li}\, h_i = \overline{\overline{E}}^s_{im}\, h_m + \overline{\overline{E}}^{cs}_{ik}\, g_k$$

$$+ \left[2\overline{S}_{imr} - 2\left(\overline{M}_\gamma\right)_{imr} \right] \overset{*}{h}_m h_r - 2\left(\overline{M}_\eta\right)_{ik\ell}\, g_k\, \overset{*}{g}_\ell + \beta_D \theta \left[- \overline{B}^{10}_i \right.$$

$$+ 2\overline{B}^8_{im}\, \overset{*}{h}_m + \overline{B}^{11}_i \Bigg] - 2(\beta_P + \beta_D)\overline{B}_{ik}\, \overset{*}{g}_k + A_{Li}$$

$$i = 1, 2, \ldots N \qquad\qquad (2.17)$$

where there is no summation over i on the left hand side of Equations (2.16) and (2.17).[†]

In deriving Equations (2.16) and (2.17), the orthogonality relations for rotating beams given in Appendix A and the boundary conditions were used. The various coefficients used in the equations are generalized masses and are defined in Appendix B. The terms A_{Fi} and A_{Li} are generalised aerodynamic coefficients given by the expressions

$$A_{Fi} = \frac{\ell^2}{\Omega^2 I_b} \int_{\overline{A}}^{\overline{B}} L_z\, \eta_i\, d\overline{x}_o \qquad\qquad (2.18)$$

$$A_{Li} = - \frac{\ell^2}{\Omega^2 I_b} \int_{\overline{A}}^{\overline{B}} L_y\, \gamma_i\, d\overline{x}_o \qquad\qquad (2.19)$$

Next the aerodynamic terms will be specified. The loading terms in the z-direction and the y-direction can be obtained from Friedmann (Ref. 13).

$$L_z = a\rho_A b R U_T\, (U_T\theta - U_p) \qquad\qquad (2.20)$$

$$L_y = -a\rho_A b R \left[U_p(U_T\theta - U_p) + \frac{C_{Do}}{a} U_T^2 \right] \qquad\qquad (2.21)$$

[†] The term $\overline{S}_{imr} - \left(M_\gamma\right)_{imr}$ is usually zero.

where the velocities U_P and U_T are given by

$$U_P = \Omega \overset{*}{w} + \Omega R \left[\lambda + \mu \cos \psi \, \frac{\partial w}{\partial x_o} \right] \tag{2.22}$$

$$U_T = \Omega \overset{*}{v} + \Omega R \left[\overline{x} + \mu \sin \psi + \mu \cos \psi \, \frac{\partial v}{\partial x_o} \right] \tag{2.23}$$

The last term in Eq. (2.23) represents the component of tangential velocity due to radial flow along an elastically deformed blade. This term has been sometimes neglected even though it is not a higher order term. The additional terms due to this effect will be underlined by _ _ _ _ for future reference.

For the purposes of this study, the inflow ratio λ in Eq. (2.22) was evaluated using an expression for constant inflow ratio in hover, given by (Ref. 13)

$$\lambda = \frac{\sigma a}{16} \left[\sqrt{1 + \frac{24\theta}{\sigma a}} - 1 \right] \tag{2.24}$$

This inflow relation is equivalent to taking the induced velocity at 3/4 blade radius as representative of a constant induced velocity over the whole disk. It is clear that for forward flight one should use the expression

$$\lambda = \mu \tan \alpha_R + C_T/2 \sqrt{\mu^2 + \lambda^2} \tag{2.25}$$

However, use of this expression would have required the use of a trim procedure by which θ is changed as a function of μ. This approach was used in Ref. 13, where it was concluded that the changes dictated by such a trim procedure have the tendency to mask the effects due to forward flight. Therefore, in order to illustrate clearly the effects of forward flight, it was decided that the use of Eq. (2.24) was more convenient.

By substituting Eqs. (2.13) through (2.15), (2.22) and (2.23) into Eqs. (2.20) and (2.21), the expressions for L_z and L_y can be obtained. Carrying out the integrations in Eqs. (2.18) and (2.19) yields the generalized aerodynamic loads A_{Fi} and A_{Li}. The complete expressions for A_{Fi} and A_{Li} are given in Appendix C. The various flap coefficients $F^1, \ldots, F^{24}$ and lag coefficients $L^1, \ldots, L^{24}$ for the aerodynamic loads are defined in Appendix B.

2.3 Linearization of the Equations

The equations of motion will be linearized about a convenient equilibrium position which is chosen as the static equilibrium position in hover.[†] The equations cannot be linearized about a forward flight condition having a particular value of μ since there is no guarantee that such an equilibrium position exists as a point of _stable_ equilibrium.

The linearization is performed by writing

$$w_e = w_e^o + \Delta w_e = \eta_k g_k^o + \eta_k \Delta g_k \qquad (2.26)$$

$$v_e = v_e^o + \Delta v_e = -\left[\gamma_m h_m^o + \gamma_m \Delta h_m\right]$$

where the ^{o} superscript denotes the static equilibrium position.

From Eqs. (2.16), (2.17), (2.26) and Eqs. (C.3) and (C.4) in Appendix C

$$\overline{M}_{Fi} \, \overline{\omega}_{Fi}^2 \, g_i^o + \overline{E}_{ik}^s \, g_k^o - \overline{E}_{im}^{cs} \, h_m^o = -\overline{B}_i^1 \, (\beta_P + \beta_D)$$
$$+ \frac{\gamma}{2} \left(\frac{\ell}{R}\right)^2 \left\{F_i \theta - F_i^2 \lambda\right\} \qquad i = i,2, \ldots M \qquad (2.27)$$

$$\overline{M}_{Li} \, \overline{\omega}_{Li}^2 \, h_i^o - \overline{\overline{E}}_{im}^s \, h_m^o - \overline{\overline{E}}_{ik}^{cs} \, g_k^o = -\overline{B}_i^{10} \, \beta_D \theta + \overline{B}_i^{11} \, \beta_D \theta$$
$$+ \frac{\gamma}{2} \left(\frac{\ell}{R}\right)^2 \left\{L_i^4 \frac{C_{Do}}{a} + L_i^1 \lambda\theta - L_i^2 \lambda^2\right\}$$
$$i = 1,2, \ldots M \qquad (2.28)$$

No summation over i on the left hand side of Eqs. (2.27) and (2.28).

[†]For every case stability of the equilibrium condition in hover is automatically checked.

11

Considering the case of one elastic mode for each degree of freedom and dropping the subscripts on the flap and lag coefficients, we have

$$\left(\overline{M}_{F1}\,\overline{\omega}_{F1}^2 + \overline{E^s}\right) g_1^o - \overline{E^{cs}}\, h_1^o = -\,\overline{B}_1^1\,(\beta_P + \beta_D)$$

$$+\,\frac{\gamma}{2}\left(\frac{\ell}{R}\right)^2\left[F^1\theta - F^2\lambda\right]$$ (2.29)

$$\left(\overline{M}_{L1}\,\overline{\omega}_{L1}^2 - \overline{\overline{E^s}}\right) h_1^o - \overline{\overline{E^{cs}}}\, g_1^o = -\,\overline{B}_1^{10}\,\beta_D\theta + \overline{B}_1^{11}\,\beta_D\theta$$

$$+\,\frac{\gamma}{2}\left(\frac{\ell}{R}\right)^2\left\{L^4\,\frac{C_{Do}}{a} + L^1\lambda\theta - L^2\lambda^2\right\}$$ (2.30)

Eqs. (2.29) and (2.30) can be solved for the static equilibrium position

$$\left\{\begin{matrix} g_1^o \\ \\ h_1^o \end{matrix}\right\} = \left[\,S\,\right]^{-1}\left\{C\right\}$$

where

$$\left[S\right] = \begin{bmatrix} \overline{M}_{F1}\,\overline{\omega}_{F1}^2 + \overline{E^s} & -\,\overline{E^{cs}} \\ \\ -\,\overline{\overline{E^{cs}}} & \overline{M}_{L1}\,\overline{\omega}_{L1}^2 - \overline{\overline{E^s}} \end{bmatrix}$$ (2.32)

$$\left\{C\right\} = \left\{\begin{matrix} -\,\overline{B}_1^1\,(\beta_P + \beta_D) + \frac{\gamma}{2}\left(\frac{\ell}{R}\right)^2\left(F^1\theta - F^2\lambda\right) \\ \\ \left(\overline{B}_1^{11} - \overline{B}_1^{10}\right)\beta_D\theta + \frac{\gamma}{2}\left(\frac{\ell}{R}\right)^2\left[L^4 + \frac{C_{Do}}{a} + L^1\lambda\theta - L^2\lambda^2\right] \end{matrix}\right\}$$

Using the order of magnitude analysis in Appendix C, only generalized aerodynamic terms up to and including second order terms are retained in the flap equation. Thus Eqs. (2.16), (2.31) and Eq. (C.3) in Appendix C become

12

$$\overline{M}_{F1} \overset{**}{\Delta g}_1 + \left\{ 2\overline{M}_{F1}\overline{\omega}_{F1}\eta_{SF1} + \frac{\gamma}{2}\left(\frac{\ell}{R}\right)^2 \left[F^8 \frac{\ell}{R} + F^9\mu \frac{\ell}{R} \sin\psi - F^{24}\mu \cos\psi \frac{\ell}{R} h_1^o \right] \right\} \overset{*}{\Delta g}_1$$

$$+ \left\{ \overline{M}_{F1}\overline{\omega}_{F1}^2 + \overline{E^s} + \frac{\gamma}{2}\left(\frac{\ell}{R}\right)^2 \left[F^6\mu \cos\psi + F^7 \frac{\mu^2}{2} \sin 2\psi \right. \right.$$

$$\left. \left. - F^{23} \frac{\mu^2}{2} (1+\cos 2\psi)h_1^o \right] \right\} \Delta g_1 + \left\{ -2\overline{P}_{111} g_1^o - 2(\beta_P+\beta_D)\overline{B}_{11}^3 + \frac{\gamma}{2}\left(\frac{\ell}{R}\right)^2 \left[F^{10}2 \frac{\ell}{r} \theta \right. \right.$$

$$+ F^{11}\mu \frac{\ell}{R} 2 \sin\psi\theta - F^{11}\mu \frac{\ell}{R} \cos\psi(\beta_P+\beta_D) - F^{11}\lambda \frac{\ell}{R} - F^{14}\mu \frac{\ell}{R} \cos\psi g_1^o \left. \right] \right\} \overset{*}{\Delta h}_1$$

$$+ \left\{ -\overline{E^{cs}} + \frac{\gamma}{2}\left(\frac{\ell}{R}\right)^2 \left[F^{21} 2\mu \cos\psi\theta - F^{22}\mu\lambda \cos\psi + F^{22} \mu^2\theta \sin 2\psi \right. \right.$$

$$\left. \left. - F^{22} \frac{\mu^2}{2} (\beta_P+\beta_D)(1 + \cos 2\psi) - F^{23} \frac{\mu^2}{2} (1 + \cos 2\psi)g_1^o \right] \right\} \Delta h_1 =$$

$$\frac{\gamma}{2}\left(\frac{\ell}{R}\right)^2 \left\{ F^2\mu \left[2 \sin\psi\theta - \cos\psi(\beta_P+\beta_D) \right] + F^3 \frac{\mu^2}{2} \left[\theta(1 - \cos 2\psi) \right. \right.$$

$$\left. - \sin 2\psi(\beta_P+\beta_D) \right] - F^3\lambda\mu \sin\psi + \left[- F^6\mu \cos\psi - F^7 \frac{\mu^2}{2} \sin 2\psi \right]g_1^o$$

$$+ \left[- F^{21} 2\mu \cos\psi\theta + F^{22} \mu\lambda \cos\psi - F^{22} \mu^2\theta \sin 2\psi \right. \qquad (2.34)$$

$$\left. + F^{22} \frac{\mu^2}{2} (\beta_P+\beta_D)(1 + \cos 2\psi) \right] h_1^o + \left[F^{23} \frac{\mu^2}{2} (1 + \cos 2\psi) \right] g_1^o h_1^o \right\}$$

From the order of magnitude analysis in Appendix C, only generalized aerodynamic terms up to and including third order terms are kept in the lag equation. Therefore, from Eqs. (2.17), (2.31) and Eq. (C.4) in Appendix C, one has

$$\overline{M}_{L1} \overset{**}{\Delta h}_1 + \left\{ 2M_{L1}\overline{\omega}_{L1}\eta_{SL1} + h_1^o\left(-2\overline{S}_{111} + 2\overline{M}_{Y_{111}}\right) - 2\beta_D\theta \ \overline{B}^8 \right.$$

$$+ \frac{\gamma}{2}\left(\frac{\ell}{R}\right)^2 \left[L^{13}\mu \cos\psi(\beta_P+\beta_D) \frac{\ell}{R} \theta + L^{13} 2\mu \sin\psi \frac{\ell}{R} \frac{C_{Do}}{a} + L^{14} 2 \frac{\ell}{R} \frac{C_{Do}}{a} \right.$$

$$\left. \left. + L^{13}\lambda \frac{\ell}{R} \theta + L^{16}\mu \cos\psi \frac{\ell}{R} \theta g_1^o \right] \right\} \overset{*}{\Delta h}_1 + \left\{ \overline{M}_{L1}\overline{\omega}_{L1}^2 - \overline{\overline{E^s}} + \frac{\gamma}{2}\left(\frac{\ell}{R}\right)^2 \left[L^{20}\mu\lambda \cos\psi\theta \right. \right.$$

13

$$+ \ L^{20} \ \frac{\mu^2}{2} \ (\beta_P + \beta_D) \theta (1 + \cos \ 2\psi) + L^{20} \mu^2 \ \frac{C_{Do}}{a} \ \sin \ 2\psi + L^{23} \ 2\mu \ \cos\psi \ \frac{C_{Do}}{a}$$

$$+ \ L^{21} \ \frac{\mu^2}{2} \ (1 + \cos \ 2\psi) \theta \ g_1^o \Bigg] \Bigg\} \ \Delta h_1 + \Bigg\{ 2\bar{M} \eta_{111} \ g_1^o + 2(\beta_P + \beta_D) \overline{B_{11}^7} + \frac{\gamma}{2} \left(\frac{\ell}{R} \right)^2 \Bigg[-L^7 \ \frac{\ell}{R} \ \theta$$

$$- \ L^8 \ \frac{\ell}{R} \ \mu \ \sin\psi\theta + L^8 2\mu \ \frac{\ell}{R} \ \cos\psi (\beta_P + \beta_D) + L^8 2\lambda \ \frac{\ell}{R} + L^{17} 2 \ \frac{\ell}{R} \ \mu \ \cos\psi \ g_1^o$$

$$+ \ L^{22} \ \frac{\ell}{R} \ \mu \ \cos\psi \ h_1^o \Bigg] \Bigg\} \ \Delta g_1^* + \Bigg\{ - \overline{\overline{E^{cs}}} + \frac{\gamma}{2} \left(\frac{\ell}{R} \right)^2 \Bigg[- L^{10} \mu \ \cos\psi\theta$$

$$- \ L^{11} \ \frac{\mu^2}{2} \ \sin \ 2\psi\theta + L^{11} \mu^2 \ (\beta_P + \beta_D) \ (1 + \cos \ 2\psi) + L^{11} \ 2\lambda\mu \ \cos\psi$$

$$+ \ L^{24} \ \mu^2 (1 + \cos \ 2\psi) g_1^o + L^{21} \ \frac{\mu^2}{2} \ (1 + \cos \ 2\psi) \theta h_1^o \Bigg] \Bigg\} \ \Delta g_1 =$$

$$\frac{\gamma}{2} \left(\frac{\ell}{R} \right)^2 \Bigg\{ - L^2 \ \frac{\mu^2}{2} \ (\beta_P + \beta_D)^2 \ (1 + \cos \ 2\psi) + L^2 \ \frac{\mu^2}{2} \ \frac{C_{Do}}{a} \ (1 - \cos \ 2\psi) + \Bigg[L^1 \mu (\beta_P + \beta_D) \theta$$

$$- \ L^2 \lambda 2\mu (\beta_P + \beta_D) \Bigg] \cos\psi + \Bigg[L^1 2\mu \ \frac{C_{Do}}{a} + L^2 \lambda\mu\theta \Bigg] \sin\psi + \Bigg[L^2 \ \frac{\mu^2}{2} \ (\beta_P + \beta_D) \theta \Bigg] \sin \ 2\psi$$

$$+ \ L^{10} \ \mu \ \cos\psi\theta + L^{11} \ \frac{\mu^2}{2} \ \sin \ 2\psi\theta - L^{11} \mu^2 (\beta_P + \beta_D) (1 + \cos \ 2\psi) - L^{11} 2\lambda\mu \ \cos\psi \Bigg] g_1^o$$

$$+ \ \Bigg[- L^{20} \ \lambda\mu \ \cos\psi\theta - L^{20} \ \frac{\mu^2}{2} \ (\beta_P + \beta_D) \theta (1 + \cos \ 2\psi) - L^{20} \ \mu^2 \ \frac{C_{Do}}{a} \ \sin \ 2\psi$$

$$- \ L^{23} \ 2\mu \ \cos\psi \ \frac{C_{Do}}{a} \Bigg] h_1^o + \Bigg[- L^{24} \ \frac{\mu^2}{2} \ (1 + \cos \ 2\psi) \Bigg] g_1^{o2}$$

$$+ \ \Bigg[- L^{21} \ \frac{\mu^2}{2} \ (1 + \cos \ 2\psi) \theta \Bigg] g_1^o \ h_1^o \Bigg\} \tag{2.35}$$

The third order terms in the lag equation are underlined by _____ for future reference. Also, the radial flow terms are underscored with _ _ _ _ _.

Eqs. (2.34) and (2.35) are a system of coupled linear periodic equations under the influence of periodic forcing. The periodicity in the coefficients

14

and the forcing are due to the effects of forward flight. The equations are coupled through the aerodynamic, inertia and stiffness terms.

Furthermore, for mathematical convenience the equations of motion have to be transformed into a system of first order equations. This is achieved by making the following substitutions.

$$\Delta \overset{*}{g}_1 = y_1$$

$$\Delta g_1 = y_2 \tag{2.36}$$

$$\Delta \overset{*}{h}_1 = y_3$$

$$\Delta h_1 = y_4$$

Thus, the equations of motion in their final form can be written as

$$\overset{*}{\underset{\sim}{y}} = \underset{\sim}{A}(\psi) \underset{\sim}{y} + \underset{\sim}{f}(\psi) \tag{2.37}$$

Where $\underset{\sim}{A}$ is a 4 x 4 matrix and $\underset{\sim}{f}$ is a column matrix. The elements of both are defined in Appendix C.

The equations of motion (2.37) will have a different form for the normal and reversed flow regions. The representation of the reversed flow together with its effect on the form of Equation (2.37) is described in Appendix D.

MATHEMATICAL METHODS FOR DETERMINING
THE STABILITY OF
LINEAR PERIODIC SYSTEMS

3.1 Introduction

This section will consist of a brief summary of the methods available

for obtaining the solutions of homogeneous systems of linear differential

equations with periodic coefficients. In general such a system is governed

by the following set of equations

$$\overset{*}{\underset{\sim}{y}} = \underset{\sim}{A}(\psi) \, \underset{\sim}{y} \tag{3.1}$$

Where $\underset{\sim}{y}$ is the state variable column matrix and $\underset{\sim}{A}(\psi)$ is an n x n

periodic matrix whose elements have a common period denoted by T, thus

$$\underset{\sim}{A}(\psi+T) = \underset{\sim}{A}(\psi) \tag{3.2}$$

The problem of determining the stability of such a system has been

considered in the literature associated with various fields:

(a) mathematics (Refs. 14-16)

(b) linear control system theory (Refs. 18-20)

(c) dynamic stability or parametric excitation problems (Refs. 21-25)

(d) structural dynamics problems related to helicopter rotor blade dynamics (Refs. 1, 5, 6, 10, 26-29)

Unfortunately, there seems to be a considerable lack of communication

between researchers working in these areas, which led to a considerable

amount of overlap and duplication of efforts. Therefore it is believed

that the various references mentioned above could be useful to other

researchers dealing with similar problems. It should be mentioned that

the list given above is far from complete and a complete review of the

bibliography dealing with equations with periodic coefficients is beyond the scope of the present study. From these references it is evident that in the past the following methods have been used:

(a) Hill's method of infinite determinants (Refs. 21, 26 and 11)

(b) Multivariable Floquet-Liapunov theory (Refs. 5, 6, 10, 18-20, 23-25, 28)

(c) Perturbation Methods (Refs. 8, 13, 21, 22)

The first method has proved to be cumbersome and numerically inefficient. The second method is the most general one, its main drawback has been the computational effort required for evaluating the transition matrix. This can be overcome by using Hsu's method. The third method is limited to cases when the parametric excitation can be expressed in terms of some small parameter which tends to limit the generality of the method.

3.2 Multivariable Floquet-Liapunov Theory

3.2.1 The Transition Matrix and Its Properties

The solutions of a system of differential equations with periodic coefficients are closely associated with the concept of the state transition matrix, therefore it is important to start by defining this matrix.

The transition matrix, or the fundamental matrix, is a matrix whose columns contain the linearly independent solutions to Equations (3.1). Thus the transition matrix in general is written as

$$\underset{\sim}{\Phi}(\psi,\psi_o) = \left[\underset{\sim}{\phi}_1(\psi,\psi_o), \; \underset{\sim}{\phi}_2(\psi,\psi_o), \; \ldots, \; \underset{\sim}{\phi}_n(\psi,\psi_o)\right] \qquad (3.3)$$

where each of the columns in equations (3.3) satisfies Equation (3.1) with the initial conditions given by

18

$$\underset{\sim}{y}_j \ (\psi_o) = \begin{cases} 1 & j = k \\ \\ 0 & j \neq k \end{cases} \tag{3.4}$$

to yield $\underset{\sim}{\phi}_k(\psi, \psi_o)$. Thus clearly

$$\underset{\sim}{\Phi}(\psi_o, \psi_o) = \underset{\sim}{I} \tag{3.5}$$

Two important properties of the transition matrix are given below (Ref. 18)

$$\det \ \underset{\sim}{\Phi}(\psi, \psi_o) = \exp\left[\int_{\psi_o}^{\psi} \text{trace} \ \underset{\sim}{A}(\sigma) d\sigma\right] \tag{3.6}$$

$$\underset{\sim}{\Phi}(\psi, \psi_o) = \underset{\sim}{\Phi}(\psi, \psi_1) \ \underset{\sim}{\Phi}(\psi_1, \ \psi_o) \tag{3.7}$$

3.2.2 The Floquet-Liapunov Theorem and Its Consequences

Proof of the Floquet-Liapunov theorem is given in References 15 and 18, for conciseness only the theorem itself will be stated.

Floquet-Liapunov Theorem. If $\underset{\sim}{A}(\psi+T) = \underset{\sim}{A}(\psi)$ then the transition matrix associated with Equation (3.1) can be written as

$$\underset{\sim}{\Phi}(\psi, \psi_o) = \underset{\sim}{P}^{-1}(\psi) e^{\underset{\sim}{R}(\psi - \psi_o)} \underset{\sim}{P}(\psi_o) \tag{3.8}$$

where

$$\underset{\sim}{P}(\psi+T) = \underset{\sim}{P}(\psi) \tag{3.9}$$

and $\underset{\sim}{R}$ is a constant matrix.

It can be shown that in general (Refs. 15 and 18)

$$e^{\underset{\sim}{R}T} = \underset{\sim}{C} = \underset{\sim}{\Phi}(T, 0) \tag{3.10}$$

where $\underset{\sim}{C}$ is also a constant matrix. Furthermore $\underset{\sim}{P}(\psi)$ is given by

$$\underset{\sim}{P}^{-1}(\psi) = \underset{\sim}{\Phi}(\psi, 0) e^{-\underset{\sim}{R}\psi} \tag{3.11}$$

The most important consequences of this theorem are

(a) Knowledge of the transition matrix over the period

19

$0 \leq \psi \leq T$ determines the solution to Equation (3.1) everywhere because from Equations (3.7) and (3.10)

$$\Phi(\psi+T,0) = \Phi(\psi,0)e^{RT} \qquad (3.12)$$

and in general

$$\Phi(\psi+sT,0) = \Phi(\psi,0) \left(e^{RT}\right)^s \qquad (3.13)$$

where s is any integer and $0 \leq \psi \leq T$.

Therefore using Equation (3.11) $P(\psi)$ is determined everywhere.

(b)   Knowledge of the transition matrix at the end of the period determines the stability of the system. From Equation (3.10) the transition matrix at $\psi = T$ clearly determines both C and R. Here two cases need to be considered.

<u>Case (1)</u>   The matrix C had n-independent eigenvectors associated with n-distinct eigenvalues. For this case this also means that R has n-independent eigenvectors, therefore from elementary linear algebra a similarity transformation can be found such that

$$Q^{-1} R Q = \lambda \qquad (3.14)$$

where the columns of Q are the n-linearly independent eigenvectors of R and λ is a diagonal matrix whose elements are the eigenvalues of R. Combining equations (3.10) and (3.14) and using the definition of the matrix exponential (Ref. 15) one has

$$e^{RT} = Qe^{\lambda T} Q^{-1} = C$$

or

$$e^{\lambda T} = \Lambda = Q^{-1} C Q = Q^{-1} \Phi (T,0)Q \qquad (3.15)$$

where Λ is a diagonal matrix containing the eigenvalues of the transition matrix at the end of one period. The eigenvalues of $\Phi (T,0)$ or the charac-

20

teristic multipliers are related to the eigenvalues of $\underset{\sim}{R}$, denoted characteristic exponents, through the relation

$$e^{\lambda_k T} = \Lambda_k \qquad k = 1, 2, \ldots \eta \qquad (3.16)$$

Clearly λ_k and Λ_k are both complex quantities in general, thus

$$\lambda_k = \zeta_k + i\omega_k \qquad (3.17)$$

$$\Lambda_k = \Lambda_{kR} + i\Lambda_{kI} \qquad$$

from which

$$\zeta_k = \frac{1}{2T} \ln \left[\Lambda_{kR}^2 + \Lambda_{kI}^2\right] \qquad (3.18)$$

$$\omega_k = \frac{1}{T} \tan^{-1} \frac{\Lambda_{kI}}{\Lambda_{kR}} \qquad (3.19)$$

the quantity ω_k can be determined according to the Floquet-Liapunov theory only within an integer multiple of the nondimensional period.

The stability criteria for the system is related to the eigenvalues of $\underset{\sim}{R}$ or the real part of the characteristic exponents ζ_k . The solutions of the Equation (3.1) approach zero as $\psi \to \infty$ if

$$| \Lambda_{kR}^2 + \Lambda_{kI}^2 | < 1 \qquad \text{or} \qquad \zeta_k < 0 \qquad k = 1, 2, \ldots, n \quad (3.20)$$

Case (2) The eigenvalues are not distinct anymore. In this case instead of finding a similarity transformation which transforms R into diagonal form, a similarity transformation can be used which transforms $\underset{\sim}{R}$ into the Jordan canonical form, this case is treated in Reference 15.

3.3 Methods for Calculating the Transition Matrix

3.3.1 General

From the description given in the previous sections it is clear that in order to obtain the solutions for a periodic system using the Floquet-Liapunov theorem one has to evaluate the transition matrix over one period.

21

This can be done using the methods described in the following sections.

3.3.2 Direct Numerical Integration

This straightforward method, which has been used in Refs. 6 and 28 is based upon equations (3.3) and (3.4). The various columns of the transition matrix are evaluated by direct numerical integration of the equations of motion, Equations (3.1), using a fourth order Runge-Kutta method, with the initial conditions specified by Equations (3.4).

3.3.3 Hsu's Method for Evaluating the Transition Matrix

In a recent series of papers, Hsu (Refs. 23-25) has developed various methods for approximating the transition matrix during one period; the most efficient one consists of approximating the periodic matrix $\underset{\sim}{A}(\psi)$ by a series of step functions, this method can be considered to be the generalization of the "rectangular ripple" (Ref. 1) method to multidimensional systems. The method consists of evaluating the state transition matrix by dividing a period into a number of equal parts and considering the equations over each interval to be a set of constant coefficient equations. Due to the fact that the method is new and numerically efficient a description of its essential aspects is given below.

Each period T is divided into K intervals denoted by

$$\psi_k, \quad k = 0, 1, 2 \ldots K, \quad \text{with } 0 = \psi_0 < \psi_1 < \ldots . \psi_K = T.$$

The kth interval $[\psi_{k-1}, \psi_k]$ is denoted by τ_k and its size by $\Delta_k = \psi_k - \psi_{k-1}$. In the kth interval the periodic coefficient matrix $\underset{\sim}{A}(\psi)$ is replaced by a constant matrix $\underset{\sim}{C}_k$ which is defined by

$$\underset{\sim}{C}_k = \underset{\sim}{A}(\xi_k) \qquad \xi_k \in \tau_k \qquad (3.21)$$

$$\underset{\sim}{C}_k = \frac{1}{\Delta_k} \int_{\psi_{k-1}}^{\psi_k} \underset{\sim}{A}(r) \, dr$$

Thus the actual system, Eq. (3.1), is approximated by an approximate system

$$\overset{*}{\underset{\sim}{x}}(\psi,k) = \underset{\sim}{C}(\psi;k)\ \underset{\sim}{x}(\psi;k) \tag{3.22}$$

where

$$\underset{\sim}{x}(0;k) = \underset{\sim}{C}$$

and

$$\underset{\sim}{C}(\psi;k) = \sum_{m=-\infty}^{\infty}\ \sum_{k=1}^{k}\ \underset{\sim}{C}_{k}[U(\psi-sT-\psi_{k-1})-U(\psi-sT-\psi_{k})] \tag{3.23}$$

The elementary theory of differential equations with constant coefficients enables one to write the fundamental matrix (or the transition matrix) of the system with $\underset{\sim}{\Phi}_A(0,k) = \underset{\sim}{I}$ as

$$\underset{\sim}{\Phi}_A(\psi,K) = \exp\left[(\psi-\psi_{K-1})\underset{\sim}{C}_K\right]\exp(\underset{\sim}{C}_{K-1}\Delta_{K-1})\ldots.\exp(\underset{\sim}{C}_1\Delta_1) \tag{3.24}$$

and the growth matrix, or approximate transition matrix at $\psi = T$ is given by

$$\underset{\sim}{H}(K) = \exp(\Delta_K\underset{\sim}{C}_K)\ \exp(\Delta_{K-1}\underset{\sim}{C}_{K-1})\ \cdots\ \exp(\Delta_1\underset{\sim}{C}_1)_- = \prod_{i=1}^{K}\ \exp(\Delta_i\underset{\sim}{C}_i) \tag{3.25}$$

With regard to the product sign, it is understood that the order of positioning of the factors is material and that the $k^{\underline{th}}$ factor is to be placed in front of the $(k-1)^{\underline{th}}$ factor.

It is shown in Reference 25 that when $K \to \infty$

$$\underset{\sim}{x}(\psi,K) \to \underset{\sim}{y}(\psi)$$

$$\underset{\sim}{\Phi}_A(\psi,K) \to \underset{\sim}{\Phi}(\psi,o)$$

and

$$\underset{\sim}{H}(K) = \underset{\sim}{\Phi}_A(T,o) \to \underset{\sim}{\Phi}\ (T,o)$$

The basic numerical problem is therefore the efficient computation of $\underset{\sim}{H}(K)$.

Using the definition of the matrix exponential

$$\exp(\Delta_i\underset{\sim}{C}_i) = \underset{\sim}{I} + \Delta_i\underset{\sim}{C}_i + \frac{(\Delta_i\underset{\sim}{C}_i)^2}{2} + \ldots \frac{(\Delta_i\ \underset{\sim}{C}_i)^n}{n!} + \ldots \tag{3.26}$$

$$n \to \infty$$

For small time intervals $\Delta_i \to 0$ and the series in Equation (3.26) converges rapidly, and the value of the matrix exponential can be accurately approximated by a finite number of terms. Thus

$$\exp(\Delta_i \underset{\sim}{C}_i) \cong \underset{\sim}{I} + \sum_{j=1}^{J} \frac{(\Delta_i \underset{\sim}{C}_i)^j}{j!} = \exp(\Delta_i \underset{\sim}{C}_i) - \sum_{j=J+1}^{\infty} \frac{(\Delta_i \underset{\sim}{C}_i)^j}{j!} \qquad (3.27)$$

Therefore the approximate value of the growth matrix can be written as

$$\underset{\sim A}{H}(K) = \prod_{i=1}^{K} \left\{ \underset{\sim}{I} + \sum_{j=1}^{J} \frac{(\Delta_i \underset{\sim}{C}_i)^j}{j!} \right\} \qquad (3.28)$$

General error bounds for these approximations are obtained in Ref. 25, furthermore it can be shown that

$$\underset{\sim}{\Phi}(T,o) - \underset{\sim A}{H}(K) = \underset{\sim}{0} \ (\Delta^2) \qquad (3.29)$$

for $J \geq 2$.

SECTION 4

RESULTS AND DISCUSSION

4.1 Numerical Quantities Used in the Calculations

In computing the numerical results the following assumptions were made:

Mass and stiffness distribution was assumed to be constant along the span of the blade.

Two different kinds of mode shapes were used:

(a) For the cases when essentially only a study of the trends or properties of the numerical methods (i.e. numerical experimentation) was conducted, the mode shapes in flap and lag were both approximated by the first nonrotating assumed mode shape (Ref. 13)

$$\eta_1 = \gamma_1 = (-\frac{1}{3}) [1-4\bar{x}_0 - (1-\bar{x}_0)^4] \qquad (4.1)$$

This equation satisfies all the boundary conditions of the problem. When an assumed mode shape is used the elastic coupling effect as represented by Equations (E.5) through (E.8) was neglected.

(b) For the majority of the cases, where a parametric investigation of typical hingeless rotor blade configurations was conducted, an exact rotating mode shape in flap and lag was employed. The exact rotating mode shapes were generated by using Galerkin's method based upon five nonrotating cantilever mode shapes for each flap or lag degree of freedom. For these cases the elastic coupling effect was included. The method by which the rotating modes were obtained is essentially identical to that described in Reference 31 and the various numerical constants required were taken from Reference 32.

The flap and lag coefficients F^i, L^i and the various generalized masses defined in Appendix B were calculated using seven-point Gaussian integration. The numerical values for these coefficients were calculated for $\ell/R = 1.0$, $\overline{A} = 0.0$, $\overline{B} = 1.0$ and $\overline{e}_1 = 0$.

As mentioned before, the inflow was evaluated using Eq. (2.24). It has been shown in Reference 13 that the correct procedure would involve a trim requirement for which θ must be changed as a function of μ at a fixed value of C_T. This added complication was not considered to be worthwhile in the present trend type study.

Finally, in all the computations the following values were used:

$$C_{do} = .01; \quad a = 2\pi; \quad \sigma = 0.05$$

Various other pertinent quantities are specified on the plots.

4.2 Brief Description of the Computer Program

This section describes briefly the computational implementation of the mathematical techniques described in Section 3. As pointed out in Section 3, the method of solution is based upon the Floquet-Liapunov theorem, but the transition matrix at the end of a period is evaluated using two different approaches: (a) Direct numerical integration, (b) Hsu's method of approximating a periodic system by a series of step functions. Consequently, the two computer programs by which the results were obtained are identical except for the routine which evaluates the transition matrix.

The computational steps are outlined below:

1. The generalized masses, and generalized aerodynamic coefficients F^i, L^i are evaluated using seven point Guassian integration. In the calculation of the aerodynamic coefficients the normal and

26

reversed flow region are accounted for as described in
Appendix D.

2. The transition matrix at the end of one period is computed using
    two separate methods

    (a) Direct Numerical Integration. For this case the elements
        of the $\underset{\sim}{A}$-matrix are generated and the resulting equations are
        integrated using the fourth order Runge-Kutta method available
        in the IBM-Scientific Subroutine Package. The numerical inte-
        gration is performed four times yielding the four columns of
        the transition matrix. The time steps used were the same as
        those used for Hsu's method.

    (b) Hsu's Method. The transition matrix is evaluated using Equa-
        tion (3.28). After some numerical experimentation it was found
        that $\Delta = T/50$ gives good accuracy. The periodic part in the
        elements of the $\underset{\sim}{A}$-matrix (Appendix C) were evaluated using
        Equation (3.21) which yields

$$\frac{1}{\psi_k - \psi_{k-1}} \int_{\psi_{k-1}}^{\psi_k} \sin \psi \, d\psi = \sin\left(\psi_{kavg}\right) \frac{2}{\Delta\psi} \sin\left(\frac{\Delta\psi}{2}\right) \qquad (4.2)$$

$$\frac{1}{\psi_k - \psi_{k-1}} \int_{\psi_{k-1}}^{\psi_k} \cos \psi \, d\psi = \cos\left(\psi_{kavg}\right) \frac{2}{\Delta\psi} \sin\left(\frac{\Delta\psi}{2}\right) \qquad (4.3)$$

$$\frac{1}{\psi_k - \psi_{k-1}} \int_{\psi_{k-1}}^{\psi_k} \sin 2\psi \, d\psi = \sin\left(2\psi_{kavg}\right) \frac{1}{\Delta\psi} \sin \Delta\psi \qquad (4.4)$$

$$\frac{1}{\psi_k - \psi_{k-1}} \int_{\psi_{k-1}}^{\psi_k} \cos 2\psi \, d\psi = \cos\left(2\psi_{kavg}\right) \frac{1}{\Delta\psi} \sin \Delta\psi \qquad (4.5)$$

where $\qquad \psi_{kavg} = \dfrac{\psi_k + \psi_{k-1}}{2}$; $\Delta\psi = \psi_k - \psi_{k-1}$

27

It is apparent from these equations that for small intervals the periodic terms could be replaced by their value at the mid-point of the interval.

3. The eigenvalues of the transition matrix at the end of a period are evaluated using a Jacobi-type eigenvalue routine. The characteristic exponents are then evaluated from Equations (3.18) and (3.19). Of the four characteristic exponents obtained, two are associated with the flap degree of freedom, and two are related to the lead-lag degree of freedom. The critical advance ratio μ_c is the advance ratio for which one of ζ_k's becomes positive. The degrees of freedom are identified by tracing back their history from $\mu = 0$.

4.3 Results

The results obtained from the present study are usually given in the form of plots representing the variation of the real part of the characteristic exponent ζ_k with the advance ratio μ.

Before proceeding with the description of the results it is important to note that Figures 3 through 8 are based upon the assumed mode shapes Eq. (4.1), and in these cases the elastic coupling effect is neglected. Figures 10 through 17 have been obtained using the exact rotating mode shapes and in these cases the elastic coupling effect is included.

Figure 3 shows results for a typical case using Runge-Kutta numerical integration and Hsu's method with different orders of approximation used in calculating the state transition matrix. This plot shows that Runge-Kutta and Hsu's method using a fourth order approximation to the solution of the constant coefficient equations in each interval give

28

almost identical results. As shown, the lag degree of freedom becomes unstable for $\mu = .754$ and the frequency of oscillation is $\omega_k = 1.286$. This result clearly indicates that by neglecting the lag degree of freedom one could obtain completely incorrect stability boundaries.

Figure 4 is a plot of the C.P.U. time required on an IBM 360/91 computer to calculate the Floquet transition matrices for the four cases depicted in Fig. 3. As shown on the figure, Hsu's method, even using a fourth order approximation, is computationally much more efficient than the fourth order Runge-Kutta numerical integration scheme.

Figure 5 is a comparison of results between fourth order Runge-Kutta and Hsu's method for a case that has a relatively high value of μ_c. Again the results compare favorably even for high values of μ.

In the derivation of the equations of motion, some new terms due to the effect of radial flow were included.*

Figures 6 and 7 show the effects of the radial flow terms on the stability of the system. The effect of neglecting the radial flow terms on the real part of the characteristic exponent associated with the flap degree of freedom is illustrated in Fig. 6. Note that the radial flow terms have a stabilizing effect on the flapping motion; with the radial flow terms suppressed, the flap degree of freedom becomes unstable at $\mu = 1.33$. The effect of the radial flow terms on the lead-lag degree of freedom is illustrated by Fig. 7; as shown, without the radial flow terms the instability is completely eliminated and the system becomes unstable in flap. When the radial flow terms are included, the lag degree of freedom is the critical one and the system becomes unstable at $\mu = .754$.

---

*The radial flow terms in this discussion are those due to the under-lined term in Eq. (2.23).

This matter was pursued further to determine which radial flow term was causing the instability in the lead-lag degree of freedom. The actual destabilizing term in the equations of motion was found to be an aerodynamic coupling term. This term couples the flap motion with the lag motion in the flap equation. Its form is

$$\mu^2 \cos^2 \psi \frac{\partial w}{\partial x_o} \frac{\partial v}{\partial x_o} \tag{4.6}$$

this term is due to the $U_T U_P$ term in Equation (2.21). The term shown above is the complete nonlinear one, clearly the one retained in the equations of motion is the coupling term obtained from linearizing this expression.

It has been pointed out by Dr. K.H. Hohenemser, at a recent meeting,[*] that this term could be transformed into a constant coefficient term, if the equations of motion are rewritten in a nonrotating coordinate system such as multiblade coordinates.

As outlined in Appendix C, the $O(\varepsilon_D^3)$ aerodynamic terms associated with the lag equation were retained in the derivation. Fig. 8 shows the effect of these third order terms on the real part of the characteristic exponent associated with the lag degree of freedom plotted as a function of the advance ratio μ. Clearly the third order terms associated with damping are the relatively important ones. The third order terms associated with damping in the lag equations are underlined by _____ in element A_{33} of $\underset{\sim}{A}$, Appendix C.

Figure 9 is given for convenience. It yields the relation between the first rotating and nonrotating nondimensional flap and lag frequencies, respectively.

_____
[*] AHS/NASA-Ames Specialists Meeting on Rotorcraft Dynamics, Moffett Field, Calif., Feb. 13-15, 1974.

As mentioned, the results presented in Figs. 3 through 8 were obtained by using the assumed mode shape and neglecting the elastic coupling effect. In order to assess the effect of this assumption the typical case has also been recomputed with the exact rotating mode shape and the elastic oupling effect, the results are shown in Figure 10. From Fig. 10 it is clear that use of the exact rotating mode in flap and lag reduced the value of μ_c to μ_c = .653, when the elastic coupling is also included μ_c is further reduced to μ_c = .583. Thus, for this case, μ_c seems to be more sensitive to the type of mode shape used than to the inclusion of the elastic coupling effect. It is also interesting to note, that for this case the elastic coupling effect is destabilizing, while for hover its effect on θ_c is quite stabilizing. (Ref. 30)

It should be noted that all the results starting from Fig. 10 are based upon the exact rotating mode shapes and the elastic coupling effect is always included.

The importance of the reversed flow region is illustrated by Fig. 11. As shown, with the reversed flow region the instability occurs at a higher value of μ than without the reversed flow region. Similar trends were observed in previous studies when only the flapping motion was considered (Ref. 5), indicating that by neglecting the reversed flow region one could expect conservative results from a stability point of view. It also indicates that for this particular case the effects of reversed flow are negligible for $\mu < 0.6$ and start being important for $\mu > 0.8$.

It is also clear from Fig. 11 that the difference in μ_c due to inclusion of the reversed flow region, for $\mu = 1.0$, is approximately 7%. Thus, the approximate representation of the reversed flow region, described in Appendix D, cannot significantly affect the accuracy of the results presented in this study.

31

Previous studies (Ref. 12) dealing with the effect of viscous type of structural damping on the stability boundaries for hover indicated that this parameter has an important stabilizing effect. The effect of this parameter for forward flight is shown in Fig. 12. The stabilizing effect of structural damping in the lag degree of freedom is evident from Fig. 12 where the value of μ_c, at which the characteristic exponent associated with the lag degree of freedom becomes positive, is plotted as a function of the viscous type of structural damping in lag. It is interesting to note that this plot indicates that the greatest stabilizing effect due to damping is obtained in the range $0 < \eta_{SL1} < .02$ (2% of critical damping), after which the gain in stability tends to level off. Similar trends were also obtained from stability studies in hover.

Again in order to illustrate the sensitivity of the results to the mode shape used and the elastic coupling effect three sets of results are presented. As seen the results are mode shape dependent and inclusion of the elastic coupling effect tends to reduce the value of μ_c, at which the instability occurs.

The effect of collective pitch setting on blade stability is illustrated by Fig. 13 for the typical case $\overline{\omega}_{F1} = 1.175$ and $\overline{\omega}_{L1} = 1.28303$. As shown for a low value of collective pitch setting $\theta = 0.05$ the lag degree of freedom becomes unstable at $\mu_c = 1.435$ and $\omega_k = 1.279$. For a high value of collective pitch setting $\theta = .30$ the lag degree of freedom becomes unstable at $\mu_c = .535$ with a frequency of $\omega_k = 1.332$. Similar results have been obtained for a variety of other cases, the results are not given here for the sake of conciseness. These results consistently indicate that there is a degradation in stability in forward flight with the increase in collective pitch setting. These results also indicate

that the use of a trim procedure, such as developed in Reference 13, should be required in realistic stability calculations in forward flight. Furthermore, it seems that the assumption of nonlifting rotors used in some forward flight studies (Ref. 7) can be nonconservative.

Figure 14 illustrates the effect of the Lock number, based on normal flow, on the stability of the blade in forward flight. As shown, an increase in the value of γ tends to destabilize the blade in the lag degree of freedom. For $\gamma = 5.0$ the lag degree of freedom becomes unstable at $\mu_c = 1.425$ and $\omega_k = 1.283$, for $\gamma = 10.$ the lag degree of freedom becomes unstable at $\mu_c = .583$ and $\omega_k = 1.295$, and for $\gamma = 15.$ the lag degree of freedom becomes unstable at $\mu_c = 0.568$ and $\omega_k = 1.294$.

Hingeless helicopter blades are usually designed with a first rotating flap frequency of $1.1 \leq \overline{\omega}_{F1} \leq 1.2.$ Thus the value of $\overline{\omega}_{F1} = 1.175$ used in the numerical calculations can be considered to a representative value for this parameter. On the other hand the rotating lag frequency for hingeless blades has usually a considerable variation, therefore it is reasonable to investigate the effect of changing this parameter over a wide range such as $0.2 \leq \overline{\omega}_{L1} \leq 2.5$, the results are presented in Fig. 15. For the sake of completeness two sets of results are presented, those with the assumed mode shapes and those with the exact rotating mode shapes and the elastic coupling effect.

Two types of instabilities are shown in Fig. 15: (a) Those for which the imaginary part of the characteristic frequency is equal to 0, 1/2 or 1 indicating that the instability is directly due to the periodic coefficients in the system, for these points the appropriate number appears inside the circles or squares indicating the flutter points and

(b) Those for which ω_k has a continuous value, usually close to the rotating lag frequency, marked by letters A, B, C etc.

As can be seen from Fig. 15 there are two regions where degradation of stability can be expected with forward flight. One region is between $0.9 \leq \bar{\omega}_{L1} \leq 1.6$, while a second and much smaller region is between $0.45 < \bar{\omega}_{L1} < 0.55$. The detrimental effect of forward flight for this region has been predicted also from purely mathematical considerations (Ref. 9).

The results presented in Fig. 15 seem to indicate that at high advance ratios a soft inplane hingeless blade with $0.7 < \bar{\omega}_{L1} < .8$ will be the most stable; while for a stiff inplane hingeless blade a lag frequency of $\bar{\omega}_{L1} > 1.6$ would be the best.

Finally, it should be noted that, although the points in Fig. 15 have been connected by lines, a possibility exists that additional flutter points which could be evaluated between the calculated points may not be exactly on the lines as drawn, this is due to the periodicity of the coefficients in the equations of motion.

Previous studies have indicated that droop and preconing can significantly affect the value of θ_c at which the linear system becomes unstable in hover. It was reasonable therefore to investigate how these parameters effect the stability of the blade in forward flight.

The results for the typical case are shown in Fig. 16, for this particular combination of flap and lag frequencies μ_c is relatively insensitive to variations in β_p, while negative angles of droop seem to be stabilizing and positive angles of droop seem to be quite destabilizing.

34

The effect of the same parameters on a case with a rotating lag frequency close to $\bar{\omega}_{L1} = 1.0$ is shown in Fig. 17. In this case both droop and preconing are strongly destabilizing. Thus it is clear that the effect of these parameters is strongly related to the combination of rotating flap and lag frequencies for the particular blade configuration.

SECTION 5

CONCLUSIONS

The most important conclusions which can be drawn from this study are summarized below:

(1) Hsu's method for calculating the Floquet transition matrix at the end of a period is a powerful computational scheme which represents a significant improvement over previous methods. Compared to direct numerical integration, Hsu's method was approximately 2.5 times faster for a system of four first order equations. For higher order systems, it probably could be more efficient by one order of magnitude.

(2) Flapping instability and response studies at high advance ratios can be inaccurate and misleading due to the neglect of the lead-lag degree of freedom. The effect of the periodic coefficients on the coupled flap-lag system shows that, in general, instability can occur at lower values of advance ratios than when the flap degree of freedom is considered by itself.

(3) In addition to the instabilities associated with the periodic coefficients (i.e. with frequencies of 0, 1/2 or 1), the coupled flap-lag system has the tendency to become unstable due to an aerodynamic coupling effect associated with the radial flow terms. This instability, which has a frequency close to the rotating lag frequency of the system, usually occurs at values of μ_c much lower than those for which the flapping degree of freedom becomes unstable.

(4) The effect of the reversed flow region is negligible for $\mu < 0.4$, but it becomes quite important for $\mu > 0.8$. The approximation of the reversed flow region, outlined in Appendix D, seems to be acceptable. The approximation is better for high advance ratios.

(5) Viscous type of structural damping in the lead-lag degree of freedom has a strong stabilizing effect on the instability due to the aerodynamic coupling effect associated with the radial flow terms.

(6) The value of the collective pitch setting has a considerable effect on the value of the advance ratio at which instabilities due to the periodic coefficients or the radial flow aerodynamic coupling terms occur. An increase in collective pitch is destabilizing, therefore high advance ratio studies which do not include this effect (nonlifting rotors) may yield unconservative results.

(7) The blade Lock number has a destabilizing effect on flap-lag instability due to aerodynamic coupling effect associated with radial flow terms.

(8) The results obtained seem to indicate that certain values of rotating lag frequencies can provide improved aeroelastic performance for hingeless blades at high advance ratios.

(9) Droop and preconing can significantly affect blade stability in forward flight. The effect of these parameters is dependent upon the particular flap and lag frequencies of the blade configuration being considered.

REFERENCES

1. Horvay, G. and S.W. Yuan. "Stability of Rotor Blade Flapping Motion when the Hinges are Tilted. Generalization of the 'Rectangular Ripple' Method of Solution," _Journal of the Aeronautical Sciences_, 14(10): 583-593, October 1947.

2. Shulman, Y. "Stability of a Flexible Helicopter Rotor Blade in Forward Flight," _Journal of the Aeronautical Sciences_, 23(7): 663-670, 693, July 1956.

3. Sissingh, G. J. "Dynamics of Rotors Operating at High Advance Ratios," _Journal of the American Helicopter Society_, 13(3): 56-63, July 1968.

4. Sissingh, G.J. and W.A. Kuczynski. "Investigations on the Effect of Blade Torsion on the Dynamics of the Flapping Motion," _Journal of the American Helicopter Society_, 15(2): 2-9, April 1970.

5. Lowis, O.J. "The Stability of Rotor Blade Flapping Motion at High Tip Speed Ratios," Aeronautical Research Council, London, Reports and Memoranda No. 3544, January 1963.

6. Peters, D.A. and K.H. Hohenemser. "Application of the Floquet Transition Matrix to Problems of Lifting Rotor Stability," _Journal of the American Helicopter Society_, 16(2): 25-33, April 1971.

7. Hohenemser, K.H. and S.K. Yin. "Some Applications of the Method of Multiblade Coordinates," _Journal of the American Helicopter Society_, 17(3): 3-12, July 1972.

8. Johnson, W. "A Perturbation Solution of Rotor Flapping Stability," _AIAA 2nd Atmospheric Flight Mechanics Conference_, AIAA Paper 72-955, Palo Alto, California, September 1972.

9. Friedmann, P. and P. Tong. "Nonlinear Flap-Lag Dynamics of Hingeless Helicopter Blades in Hover and in Forward Flight," _Journal of Sound and Vibration_, 30(1): 9-32, September 8, 1973.

10. Hall, W.E. "Application of Floquet Theory to the Analysis of Rotary Wing VTOL Stability," Stanford University Center for Systems Research, Palo Alto, California, SUDDAR No. 400, February 1970.

11. Crimi, P. "A Method for Analyzing the Aeroelastic Stability of a Helicopter Rotor in Forward Flight," Rochester Applied Sciences Associates, Rochester, New York, Report RASA 68-10 (NASA-CR-1332), August 1969.

12. Friedmann, P. "Aeroelastic Instabilities of Hingeless Helicopter Blades," _AIAA 11th Aerospace Sciences Meeting_, AIAA Paper No. 73-193, Washington, D.C., January 1973.

13. Friedmann, P. and P. Tong. "Dynamic Nonlinear Elastic Stability of Helicopter Rotor Blades in Hover and Forward Flight," Aeroelastic and and Structures Research Laboratory, Department of Aeronautics and Astronautics, Massachusetts Institute of Technology, Cambridge, ASRL TR 166-3(NASA-CR-114485), June 1972.

14. Caesari, L. Asymptotic Behavior and Stability Problems in Ordinary Differential Equations, 3rd ed., Springer-Verlag, Berlin-Gottingen-Heidelberg, Germany, 1970.

15. Coddington, E.A. and N. Levinson. Theory of Ordinary Differential Equations, McGraw-Hill, New York, 1955.

16. Kaplan, Wilfred. Operational Methods for Linear Systems, Addison-Wesley, Reading, Massachusetts, 1962.

17. Erugin, N.P. Linear Systems of Ordinary Differential Equations with Periodic and Quasi-Periodic Coefficients, Academic Press, New York 1966.

18. Brockett, R.W. Finite Dimensional Linear Systems, John Wiley and Sons, New York, 1970.

19. Derusso, P.M., R.J. Roy and C.M. Close. State variables for Engineers, John Wiley and Sons, New York, 1965.

20. Zadeh, L.A. and C.A. Desoer. Linear System Theory: The State Space Approach, McGraw-Hill, New York, 1963.

21. Bolotin, Vladimir V. The Dynamic Stability of Elastic Systems, Holden-Day, San Francisco, 1964.

22. Fu, F.C. and S. Nemat-Nasser. "Stability of Solution of Systems of Linear Differential Equations with Harmonic Coefficients," AIAA Journal, 10(1): 30-36, January 1973.

23. Hsu, C.S. "Impulsive Parametric Excitation: Theory," Journal of Applied Mechanics, 39(2): 551-558, June 1972.

24. Hsu, C.S. and W.H. Cheng. "Applications of the Theory of Impulsive Parametric Excitation and New Treatments of General Parametric Excitation Problems," Journal of Applied Mechanics, 40(1): 78-86, March 1973.

25. Hsu, C.S. "On Approximating a General Linear Periodic System," to appear in the Journal of Mathematical Analysis and Applications.

26. Horvay, G. "Unstable Solutions of a Class of Hill Differential Equations," Quarterly of Applied Mathematics, 4(4): 385-396, January 1947.

27. Horvay, G. "Rotor Blade Flapping Motion," Quarterly of Applied Mathematics, 5(2): 149-167, July 1947.

28. Hohenemser, K.H. and S.K. Yin. "Concepts for a Theoretical and Experimental Study of Lifting Rotor Random Loads and Vibrations," Department of Mechanical and Aerospace Engineering, School of Engineering and Applied Science, Washington University, St. Louis, Missouri, Contract NAS 2-4151, June 1971.

29. Gockel, M.A. "Practical Solution of Linear Equations with Periodic Coefficients," Journal of the American Helicopter Society, 17(1): 2-10, January 1972.

30. Ormiston, R.A. and D.H. Hodges. "Linear Flap-Lag Dynamics of Hingeless Helicopter Rotor Blades in Hover," Journal of the American Helicopter Society, 17(2): 2-14, April 1972.

31. Yntema, R.T., "Simplified Procedures and Charts for the Rapid Estimation of Bending Frequencies of Rotating Beams," NACA Technical Note 3459, 1955.

32. Young, D., and Felgar, R.P., "Tables of Characteristic Functions Representing Normal Modes of Vibration of a Beam," Report No. 44, Bureau of Eng. Res., University of Texas, 1949.
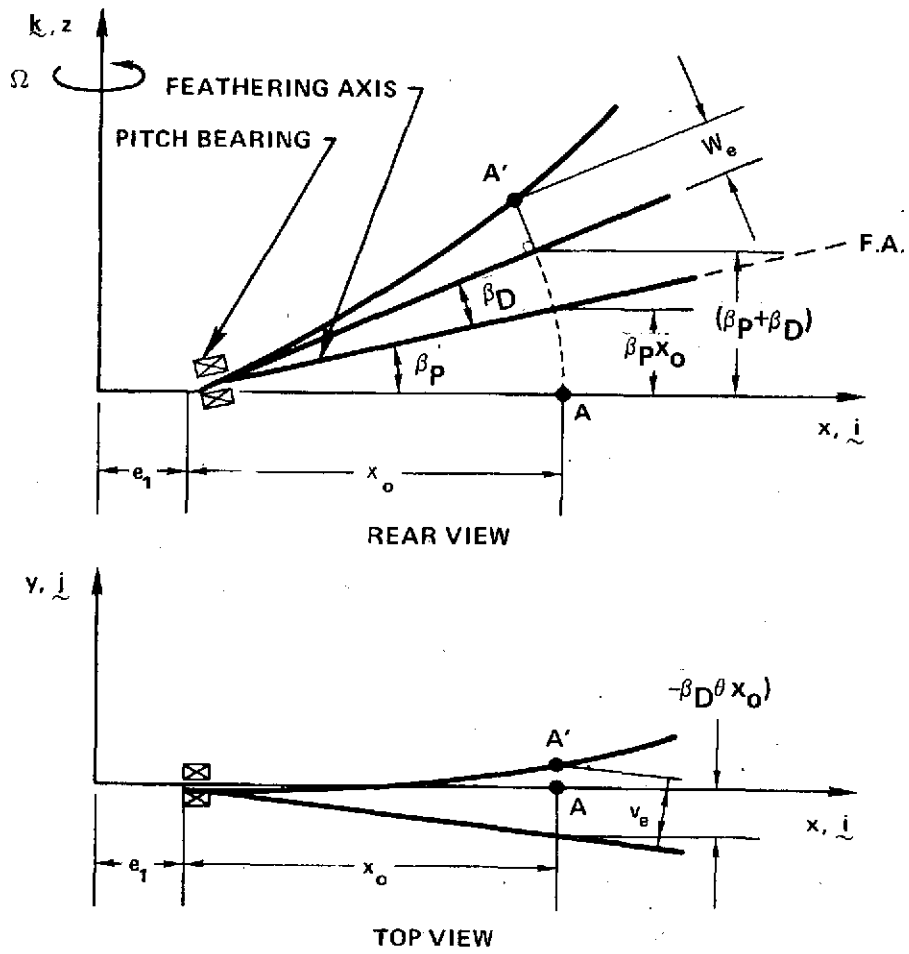
Figure 1.   Displacement Field of a Torsionally Rigid Cantilevered Blade with Droop and Preconing.
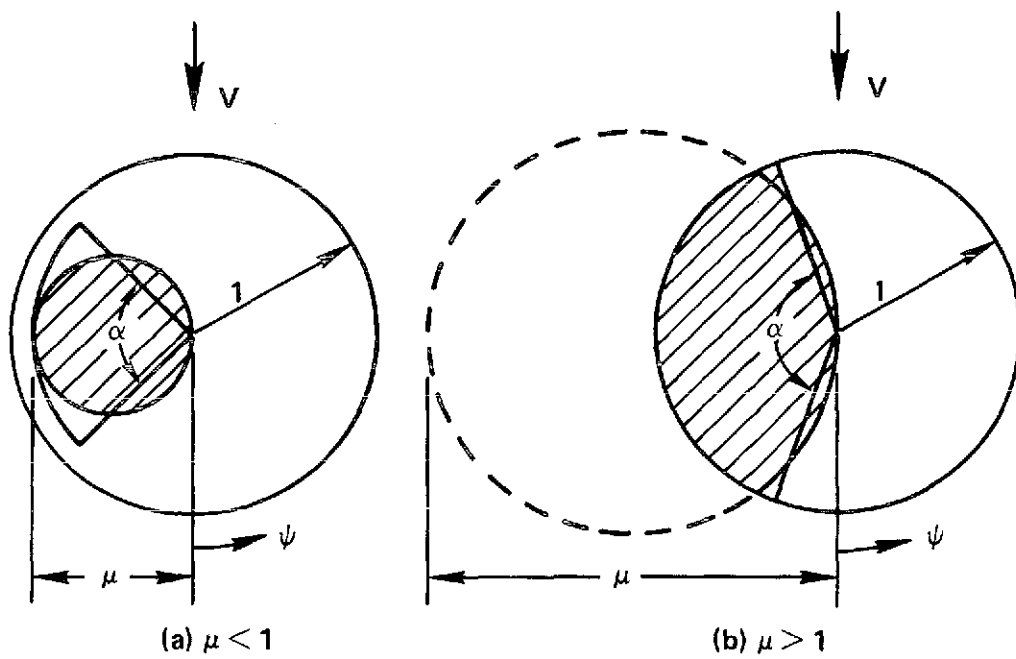
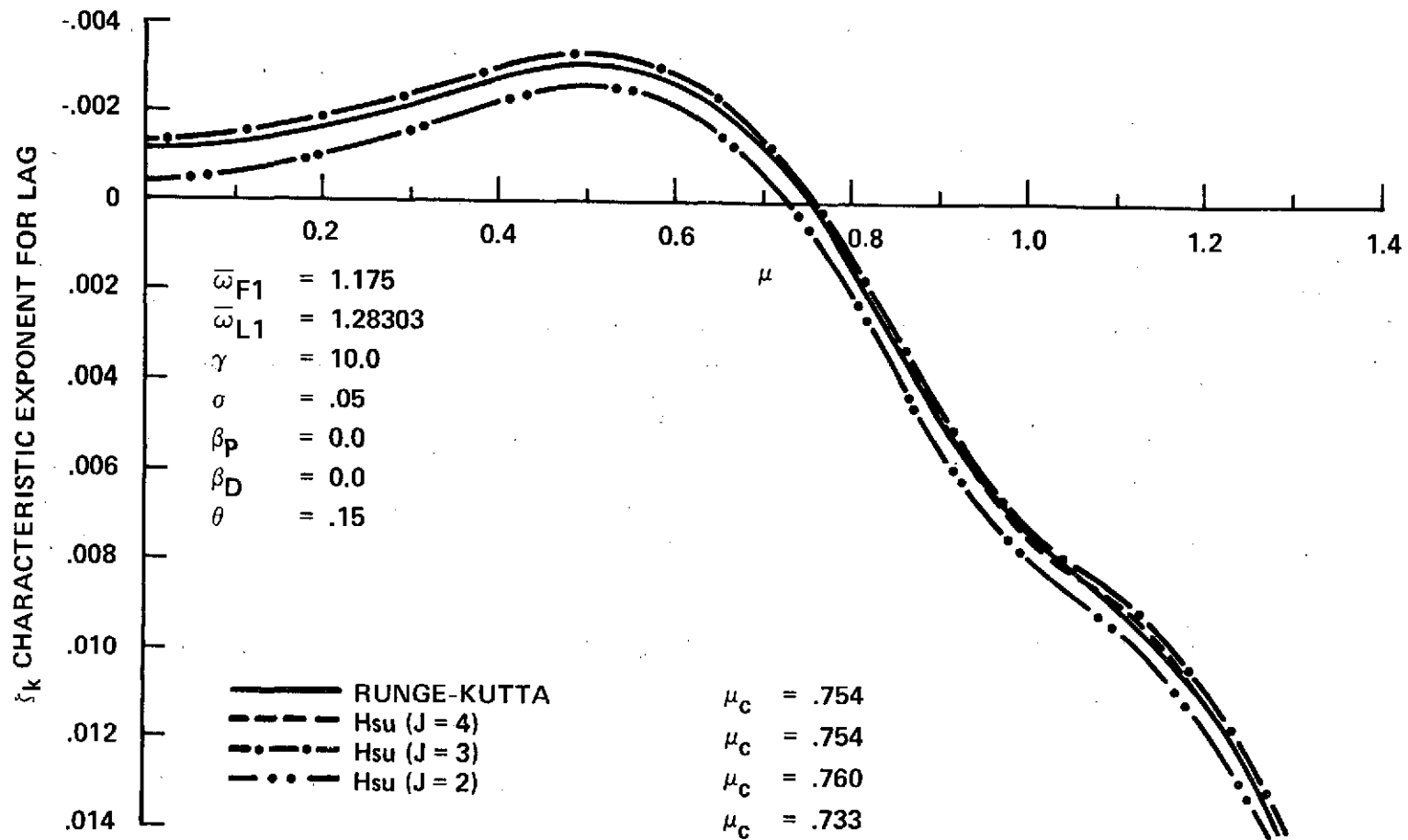Figure 2. Geometry of Approximate and Exact Reversed Flow Regions.

Figure 3. Comparison of Runge-Kutta and Hsu's Methods for a Typical Case.
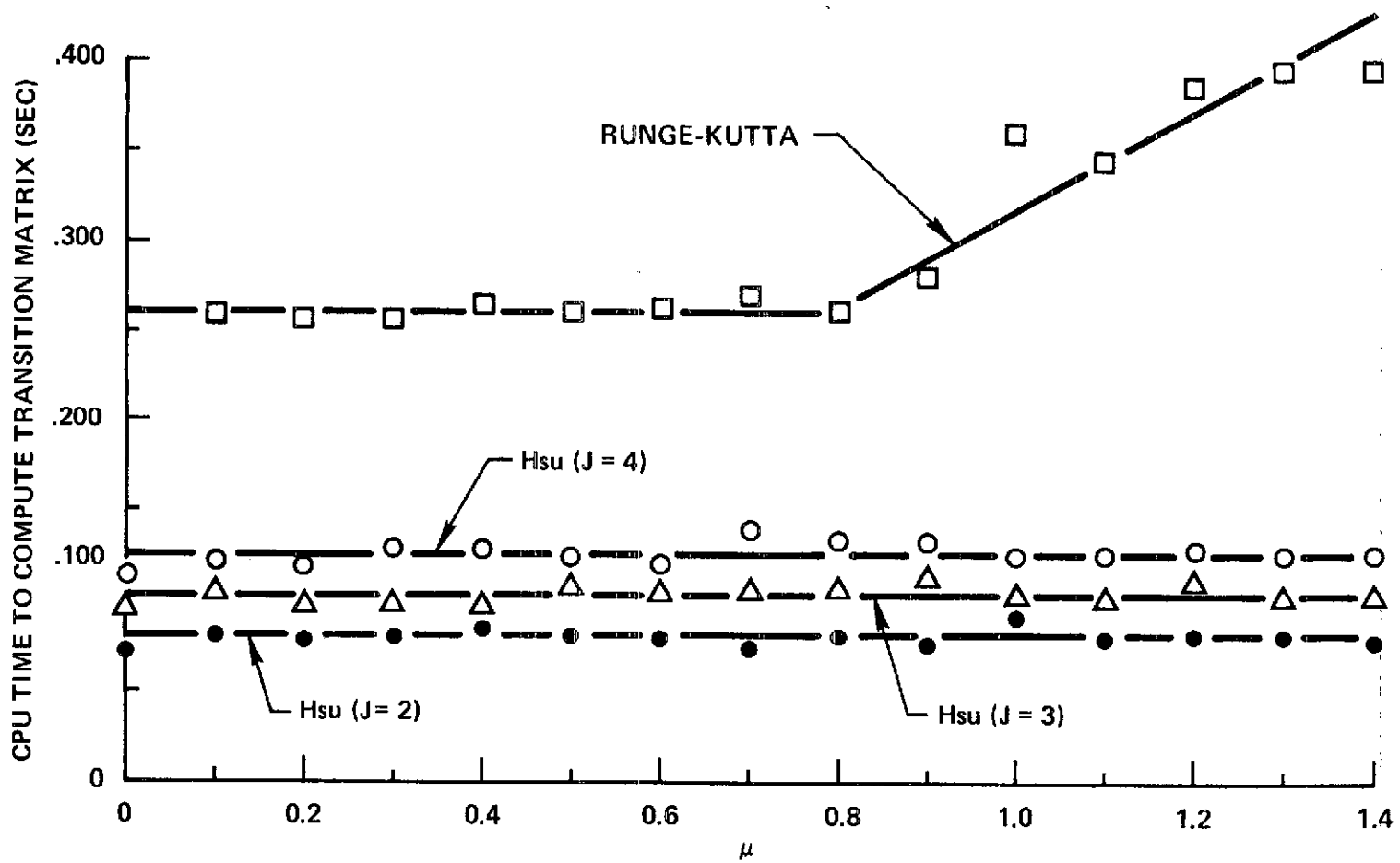
Figure 4. Variation of CPU Time to Compute Transition Matrix With Advance Ratio.
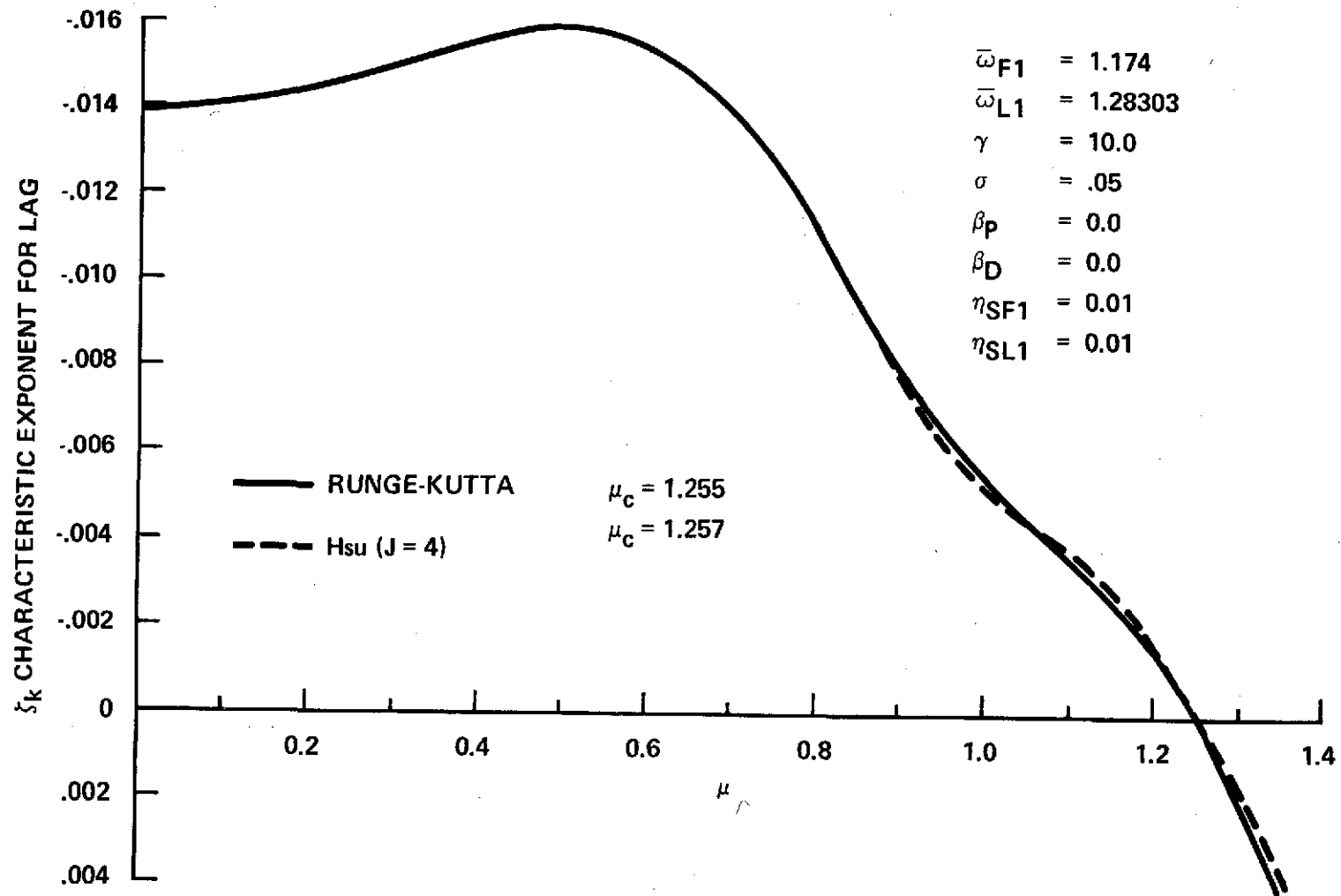
Figure 5.   Comparison of Runge-Kutta and Hsu's Methods for a Case With High μ_c.
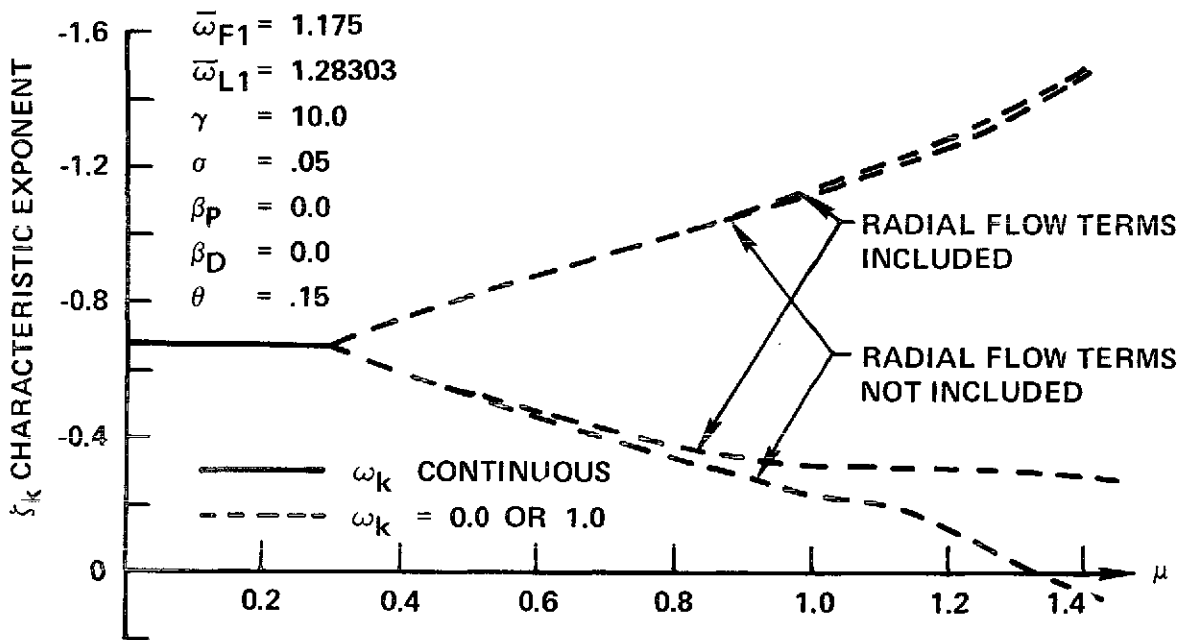
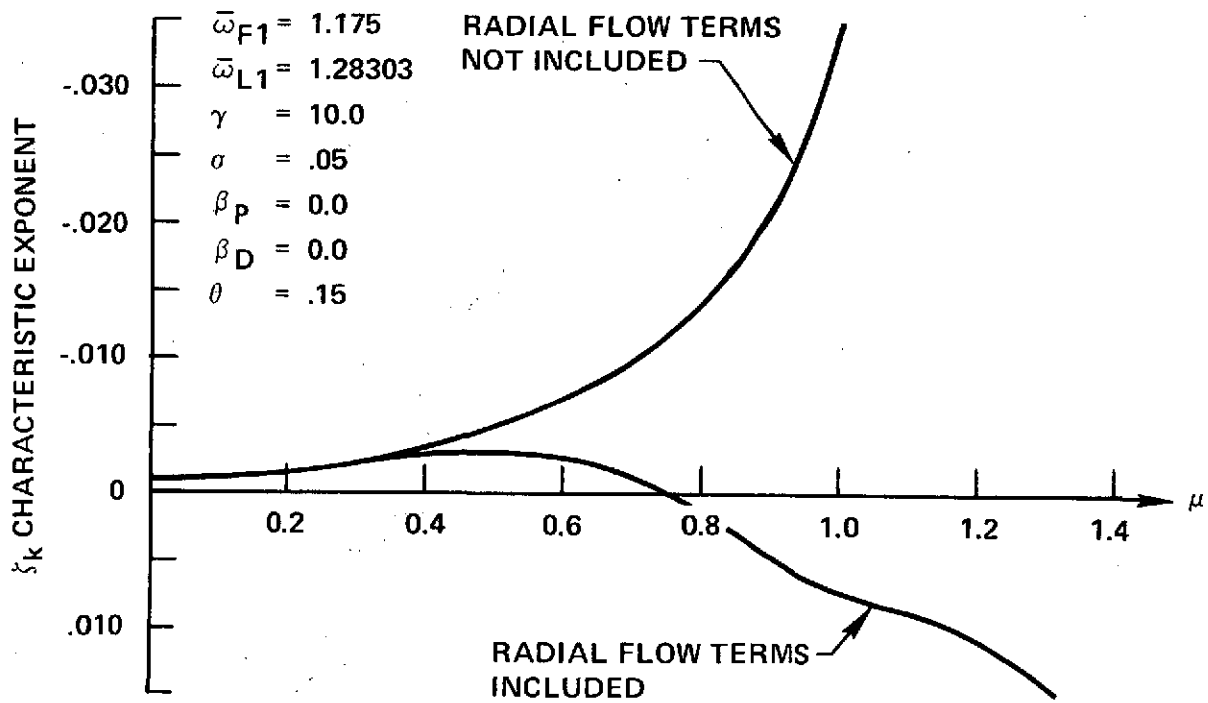Figure 6. Effect of Radial Flow Terms on Characteristic Exponent for Flap.

Figure 7. Effect of Radial Flow Terms on Characteristic Exponent for Lag.
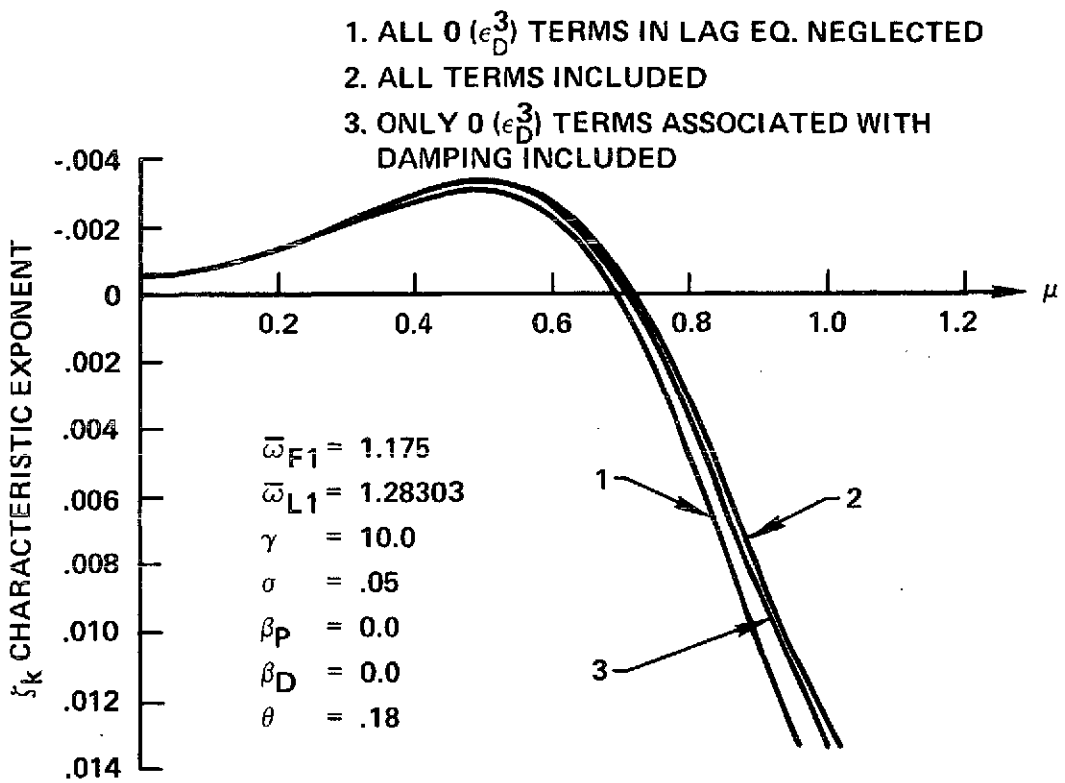
Figure 8. Effect of Third Order Terms in the Lag Equation on Characteristic Exponent for Lag.
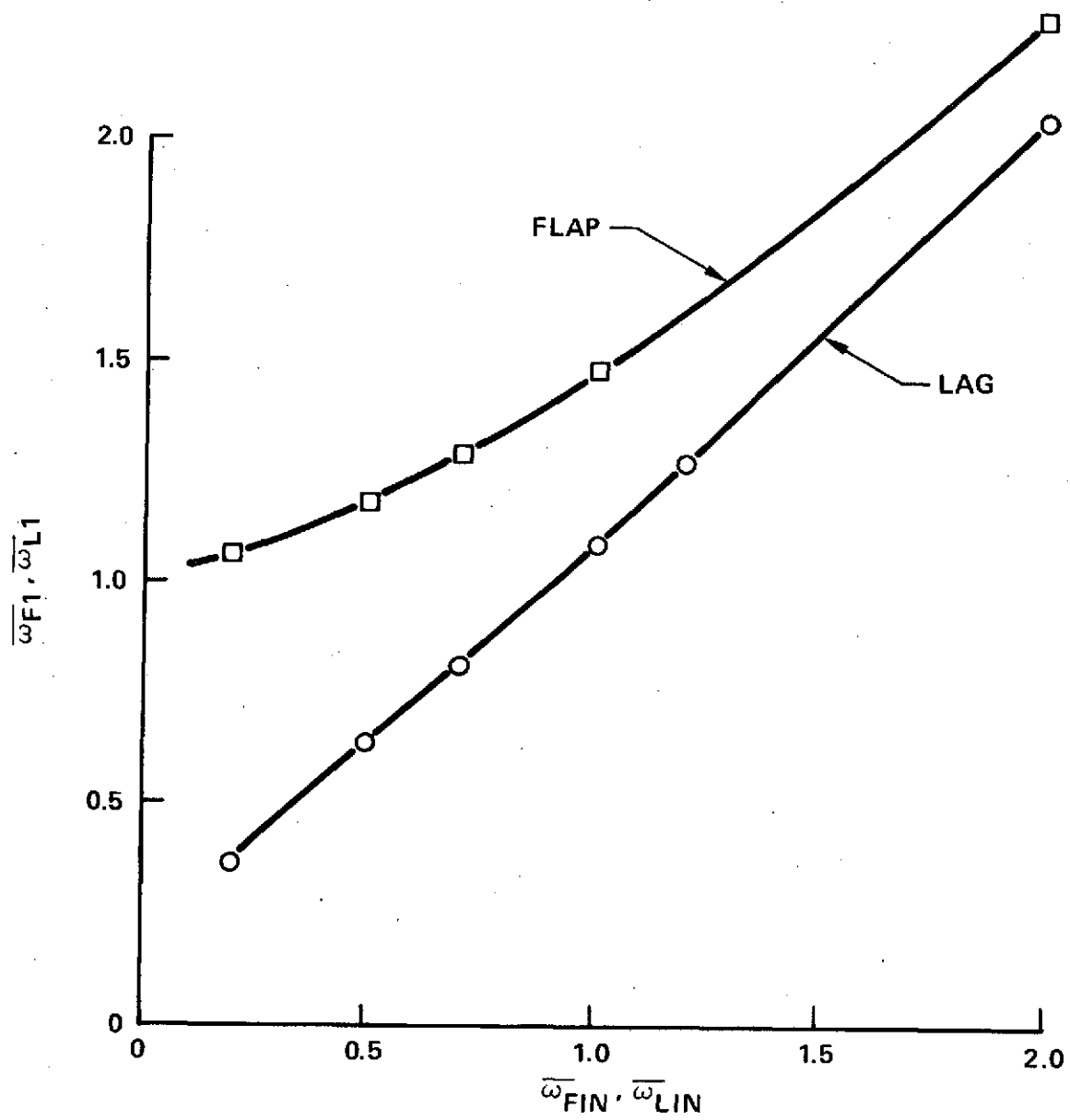
Figure 9.   Relation Between First Non-Rotating and Rotating Non-Dimensionalized Flap and Lag Frequencies.
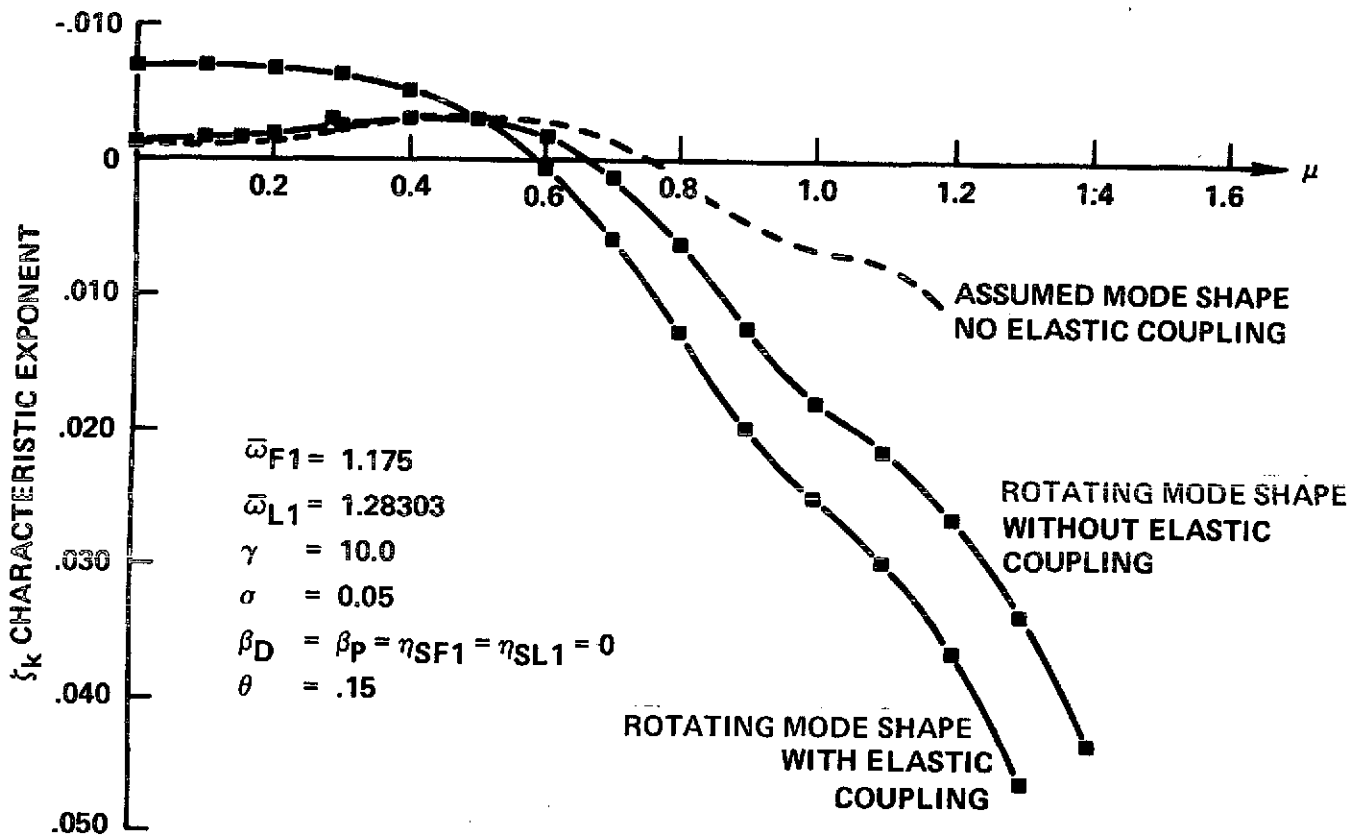
Figure 10. Effect of Exact Mode Shape and Elastic Coupling on Characteristic Exponent for Lag.
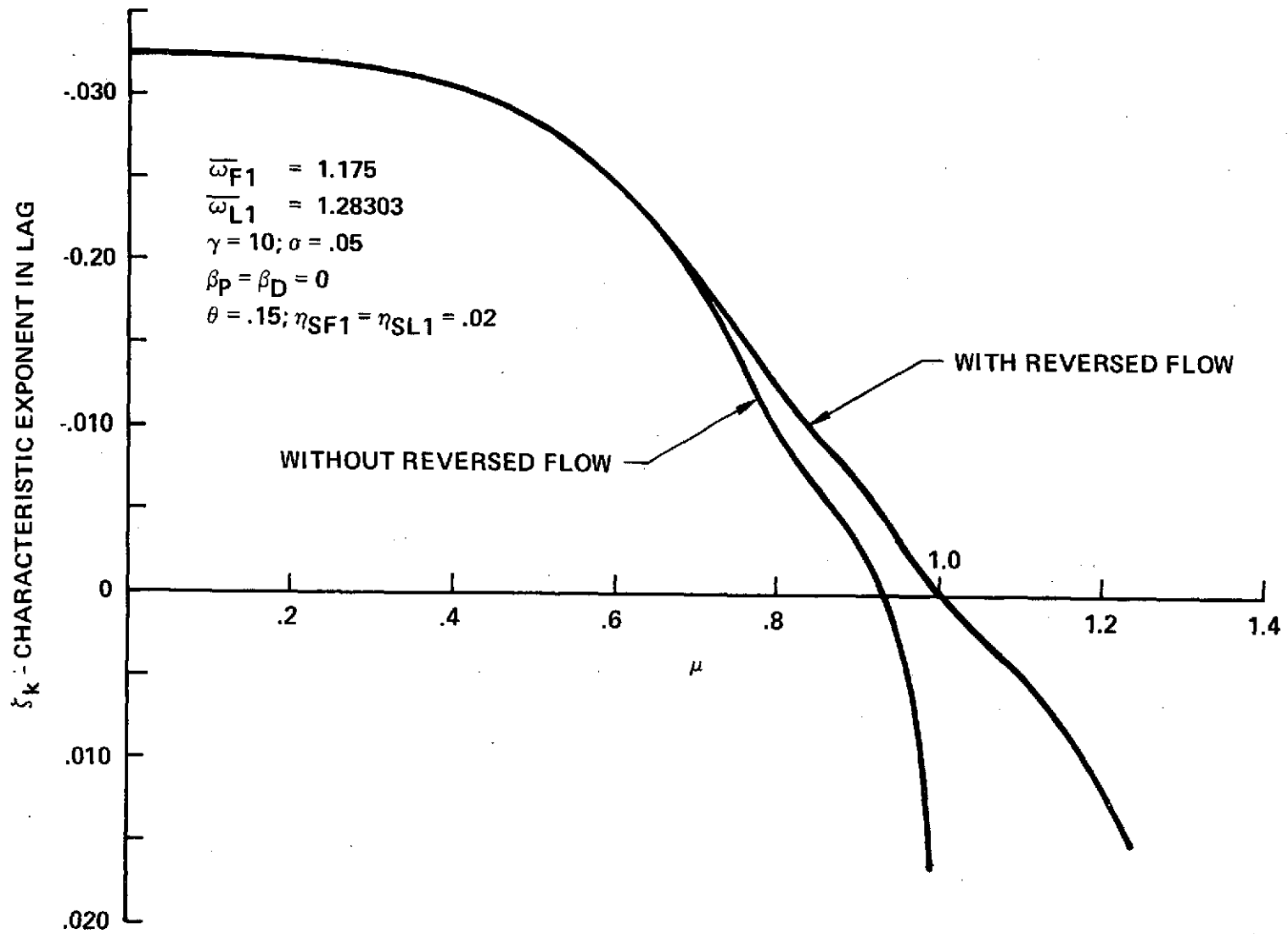
Figure 11. Effect of Reversed Flow on the Characteristic Exponent for Lag.
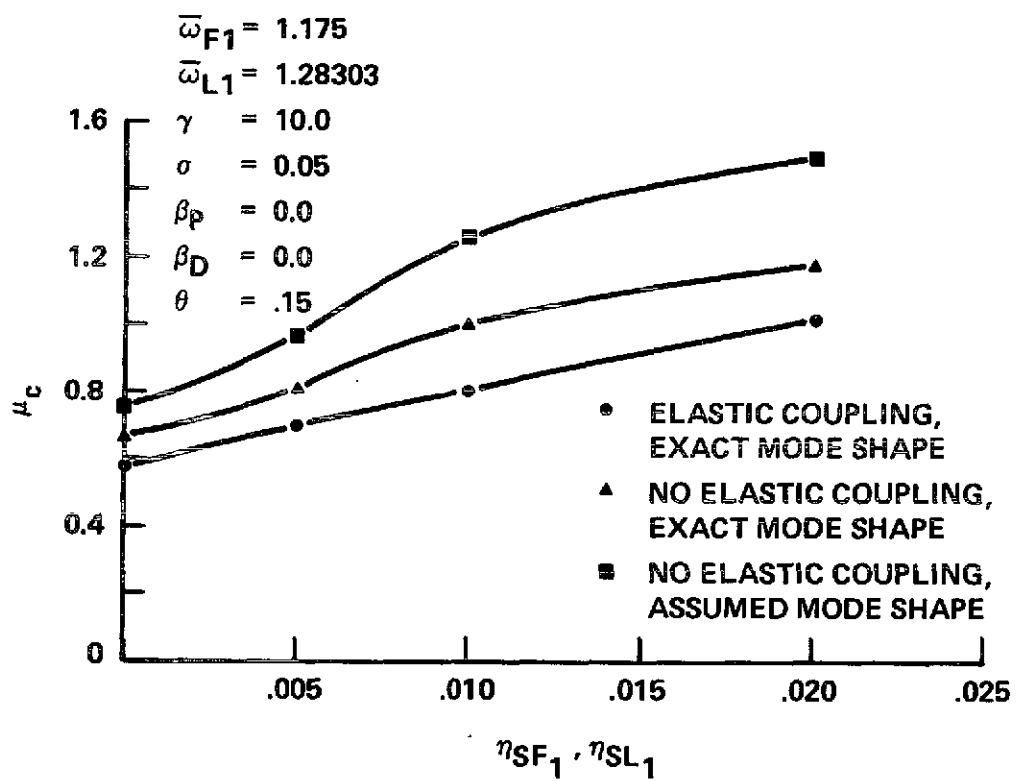
Figure 12. Effect of Viscous Structural Damping on μ_c.
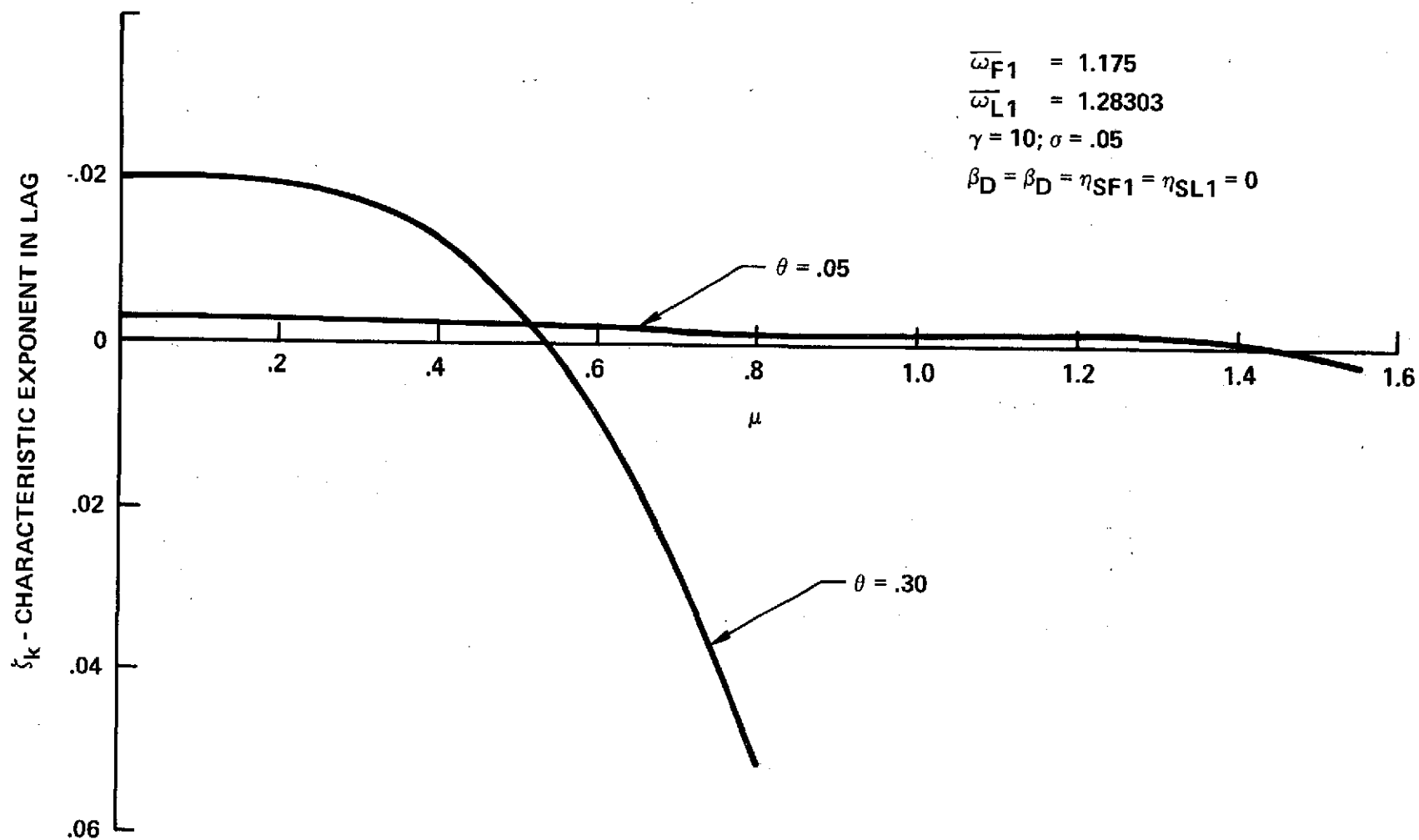
Figure 13. Effect of Collective Pitch Setting on Typical Case.
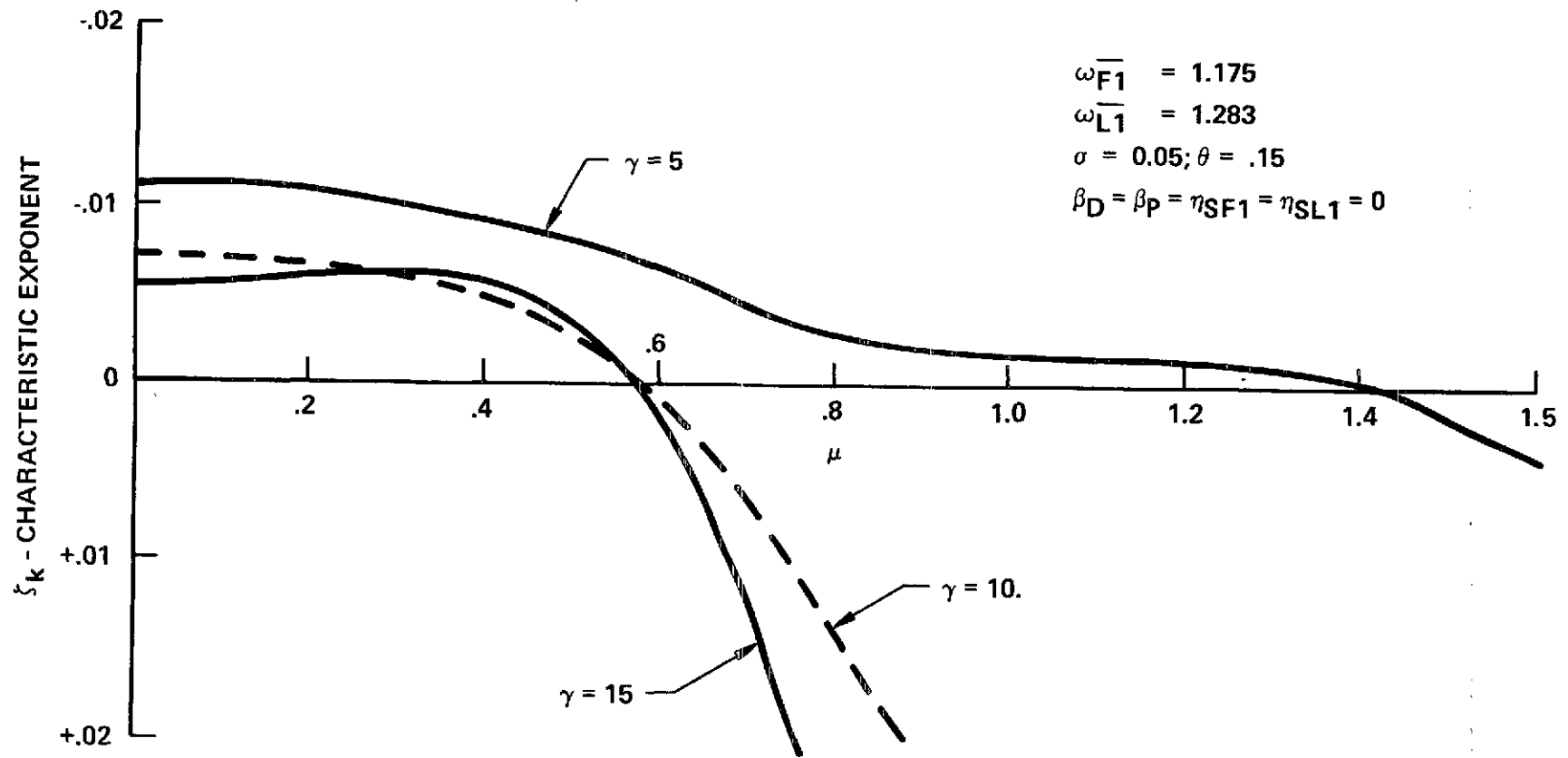
Figure 14. Effect of Lock Number on Characteristic Exponent for Lag.

Figure 15. Effect of Variation in Rotating Lag Frequency on μ_c.
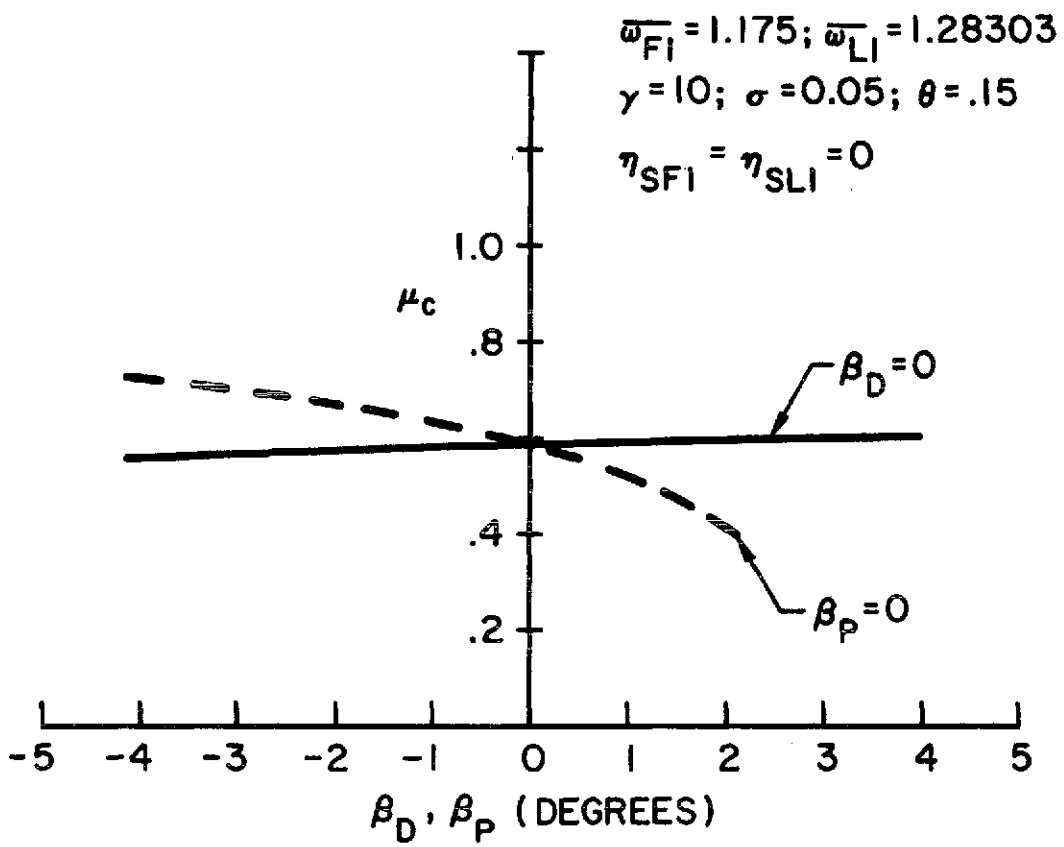
Figure 16. Effect of Droop and Preconing on μ_c for Typical Case.

$$\eta_{SFI} = \eta_{SLI} = 0$$

$$\gamma = 10; \quad \sigma = .05; \quad \theta = .15$$

$$\overline{\omega_{FI}} = 1.175; \quad \overline{\omega_{LI}} = 0.9938$$

Figure 17. Effect of Droop and Preconing on μ_c.

APPENDIX A

ORTHOGONALITY CONDITIONS

The orthogonality condition for a rotating beam vibrating out of its plane of rotation is obtained from Friedmann (Ref. 13). with $\theta = 0$

$$\frac{1}{\Omega^2 \ell} \int_0^1 (EI)_y \eta_i'' \eta_k'' \, d\bar{x}_o + \int_0^1 \eta_i' \eta_k' \left[\ell^3 \int_{\bar{x}_o}^1 m(\bar{x}_1 + \bar{e}_1) d\bar{x}_1 \right] d\bar{x}_o = 0 \qquad (A.1)$$

for $i \neq k$ and

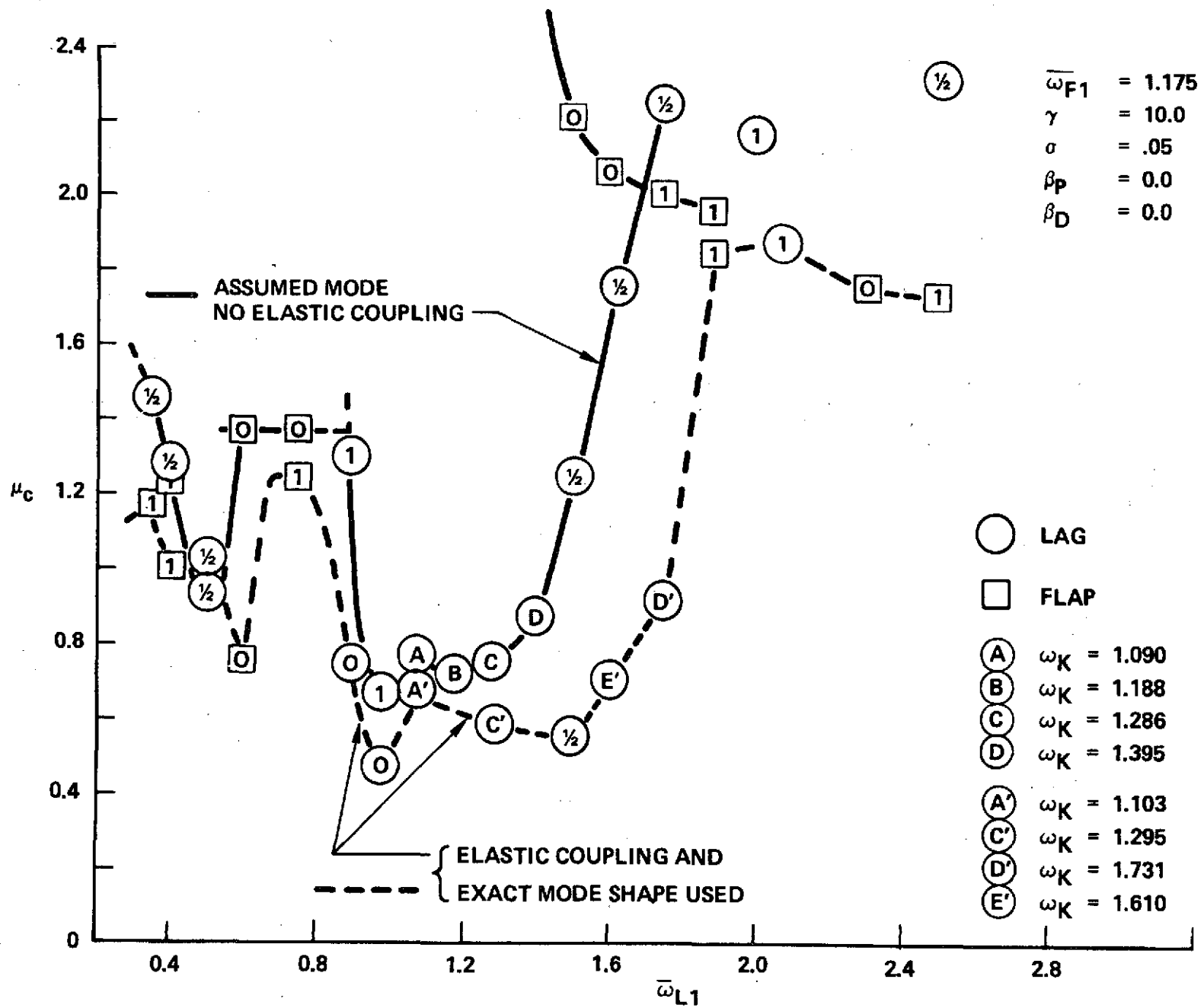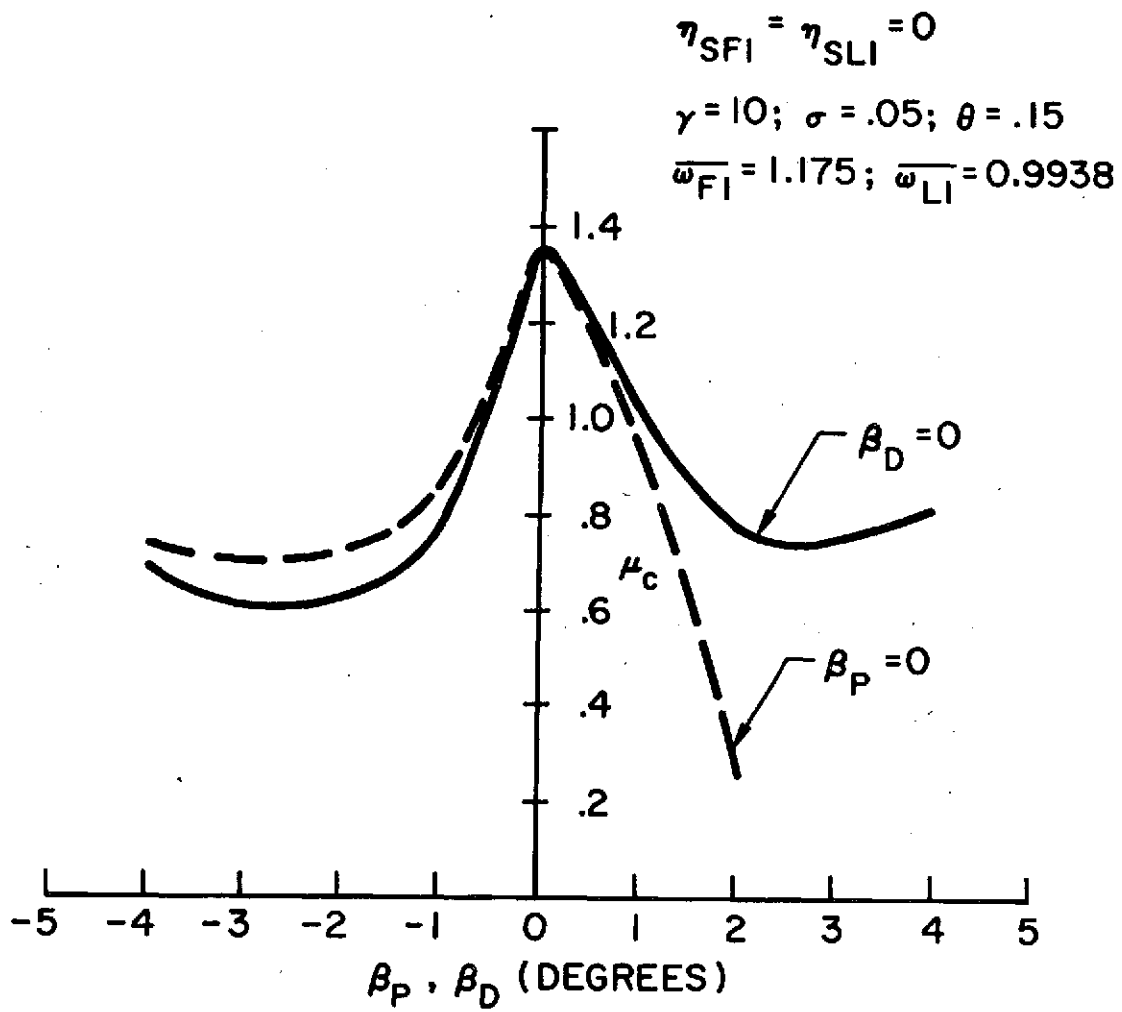$$\frac{1}{\Omega^2 \ell} \int_0^1 (EI)_y (\eta_i'')^2 \, d\bar{x}_o + \int_0^1 (\eta_i')^2 \left[\ell^3 \int_{\bar{x}_o}^1 m(\bar{x}_1 + \bar{e}_1) d\bar{x}_1 \right] d\bar{x}_o =$$

$$\frac{\ell^3 \omega_{Fi}^2}{\Omega^2} \int_0^1 m\eta_i^2 \, d\bar{x}_o \qquad \text{for} \quad i = k \qquad (A.2)$$

The orthogonality condition for a rotating beam vibrating in its plane of rotation is

$$\frac{1}{\Omega^2 \ell} \int_0^1 (EI)_z \gamma_i'' \gamma_m'' \, d\bar{x}_o + \ell^3 \int_0^1 \gamma_i' \gamma_m' \left[\int_{\bar{x}_o}^1 m(\bar{x}_1 + \bar{e}_1) d\bar{x}_1 \right] d\bar{x}_o$$

$$- \ell^3 \int_0^1 m\gamma_i \gamma_m \, d\bar{x}_o = 0 \qquad (A.3)$$

for $i \neq m$ and

$$\frac{1}{\Omega^2 \ell} \int_0^1 (EI)_z (\gamma_i'')^2 \, d\bar{x}_o + \ell^3 \int_0^1 (\gamma_i')^2 \int_{\bar{x}_o}^1 m(\bar{x}_1 + \bar{e}_1) d\bar{x}_o$$

$$- \ell^3 \int_0^1 m \gamma_i^2 \, d\bar{x}_o = \frac{\omega_{Li}^2 \ell^3}{\Omega^2} \int_0^1 m \gamma_i^2 \, d\bar{x}_o \qquad (A.4)$$

when $i = m$

These relations determine ω_{Fi}, ω_{Li}.

61

APPENDIX B

COEFFICIENTS ASSOCIATED WITH GENERALIZED MASSES,

DAMPING AND AERODYNAMIC LOADING

The non-dimensionalized general masses are

$$I_b = \ell^3 \int_0^1 m \, \bar{x}_o^2 \, d\bar{x}_o$$

$$\overline{P_{ikm}} = \ell^3 \int_0^1 \eta_i' \, \eta_k' \left(\int_{\bar{x}_o}^1 m \, \gamma_m \, \bar{x}_1 \, d\bar{x}_1 \right) d\bar{x}_o \Big/ I_b$$

$$\overline{M}_{Fi} = \ell^3 \int_0^1 m \, \eta_i^2 \, d\bar{x}_o \Big/ I_b$$

$$\overline{M}_{Li} = \ell^3 \int_0^1 m \, \gamma_i^2 \, d\bar{x}_o \Big/ I_b$$

$$\overline{C}_i = \ell^3 \int_0^1 m \, \gamma_i \, d\bar{x}_o \Big/ I_b$$

$$\overline{S}_{imr} = \ell^3 \int_0^1 \gamma_i' \, \gamma_r' \left(\int_{\bar{x}_o}^1 m \, \gamma_m \, d\bar{x}_1 \right) d\bar{x}_o \Big/ I_b$$

$$\left(M_\eta \right)_{ik\ell} = \ell^3 \left[\int_0^1 m \, \gamma_i \left(\int_0^{\bar{x}_o} \eta_k' \, \eta_\ell' \, d\bar{x}_1 \right) d\bar{x}_o \right] \Big/ I_b$$

$$\left(M_\gamma \right)_{imr} = \ell^3 \left[\int_0^1 m \, \gamma_i \left(\int_0^{\bar{x}_o} \gamma_m' \, \gamma_r' \, d\bar{x}_1 \right) d\bar{x}_o \right] \Big/ I_b$$

$$\overline{B_i^1} = \frac{\ell^3}{I_b} \int_0^1 \eta_i' \left[\int_{\bar{x}_o}^1 m(\bar{x}_1 + \bar{e}_1) \, d\bar{x}_1 \right] d\bar{x}_o$$

$$\overline{B_{im}^3} = \frac{\ell^3}{I_b} \int_0^1 \eta_i' \left[\int_{\bar{x}_o}^1 m \, \gamma_m \, d\bar{x}_1 \right] d\bar{x}_o$$

$$\overline{B_{ik}^7} = \frac{\ell^3}{I_b} \int_0^1 m\, \eta_k\, \gamma_i\, d\overline{x}_o$$

$$\overline{B_{im}^8} = \frac{\ell^3}{I_b} \int_0^1 \gamma_i \left[\int_{\overline{x}_o}^1 m\, \gamma_m\, d\overline{x}_1 \right] d\overline{x}_o$$

$$\overline{B_i^{10}} = \frac{\ell^3}{I_b} \int_0^1 \gamma_i \left[\int_{\overline{x}_o}^1 m(\overline{x}_1 + \overline{e}_1)\, d\overline{x}_1 \right] d\overline{x}_o$$

$$\overline{B_i^{11}} = \frac{\ell^3}{I_b} \int_0^1 \overline{x}_o\, m\, \gamma_i\, d\overline{x}_o$$

The viscous type of structural damping ratio is defined by

$$\eta_{SFi} = \frac{\int_0^1 \eta_i^2\, d\overline{x}_o\ g_{SF}}{\Omega I_b\ 2\overline{\omega}_{Fi}\ \overline{M}_{Fi}}$$

$$\eta_{SLi} = \frac{\int_0^1 \gamma_i^2\, d\overline{x}_o\ g_{SL}}{\Omega I_b\ 2\overline{\omega}_{Li}\ \overline{M}_{Li}}$$

Listed below are the coefficients associated with aerodynamic loads. These integrals are evaluated between the lower limit $\overline{A}$ and the upper limit $\overline{B}$ where $\overline{A}$ and $\overline{B}$ are the tip loss factors. The calculation of the aerodynamic loads in the mixed or reversed flow regions is described in Appendix D.

$$F_i^1 = \int \overline{x}^2\, \eta_i\, d\overline{x}_o \qquad\qquad L_i^1 = \int \overline{x}\, \gamma_i\, d\overline{x}_o$$

$$F_i^2 = \int \overline{x}\, \eta_i\, d\overline{x}_o \qquad\qquad L_i^2 = \int \gamma_i\, d\overline{x}_o$$

$$F_i^3 = \int \eta_i\, d\overline{x}_o \qquad\qquad L_i^4 = \int \overline{x}^2\, \gamma_i\, d\overline{x}_o$$

$$F^6_{ik} = \int \bar{x}\, \eta_i\, \eta'_k\, d\bar{x}_o \qquad\qquad L^7_i = \int \bar{x}\, \gamma_i\, \eta_k\, d\bar{x}_o$$

$$F^7_{ik} = \int \eta_i\, \eta'_k\, d\bar{x}_o \qquad\qquad L^8_{ik} = \int \gamma_i\, \eta_k\, d\bar{x}_o$$

$$F^8_{ik} = \int \bar{x}\, \eta_i\, \eta_k\, d\bar{x}_o \qquad\qquad L^{10}_{ik} = \int \bar{x}\, \gamma_i\, \eta'_k\, d\bar{x}_o$$

$$F^9_{ik} = \int \eta_i\, \eta_k\, d\bar{x}_o \qquad\qquad L^{11}_{ik} = \int \gamma_i\, \eta'_k\, d\bar{x}_o$$

$$F^{10}_{im} = \int \bar{x}\, \eta_i\, \gamma_m\, d\bar{x}_o \qquad\qquad L^{13}_{im} = \int \gamma_i\, \gamma_m\, d\bar{x}_o$$

$$F^{11}_{im} = \int \eta_i\, \gamma_m\, d\bar{x}_o \qquad\qquad L^{14}_{im} = \int \gamma_i\, \gamma_m\, \bar{x}\, d\bar{x}_o$$

$$F^{14}_{ikm} = \int \eta_i\, \eta'_k\, \gamma_m\, d\bar{x}_o \qquad\qquad L^{16}_{ikm} = \int \gamma_i\, \eta'_k\, \gamma_m\, d\bar{x}_o$$

$$F^{15}_{ikm} = \int \eta_i\, \eta_k\, \gamma_m\, d\bar{x}_o \qquad\qquad L^{17}_{ik\ell} = \int \gamma_i\, \eta'_k\, \eta_\ell\, d\bar{x}_o$$

$$F^{21}_{im} = \int \bar{x}_o\, \eta_i\, \gamma'_m \qquad\qquad L^{18}_{ik\ell} = \int \gamma_i\, \eta_k\, \eta_\ell\, d\bar{x}_o$$

$$F^{22}_{im} = \int \eta_i\, \gamma'_m\, d\bar{x}_o \qquad\qquad L^{19}_{ikm} = \int \gamma_i\, \eta_k\, \gamma_m\, d\bar{x}_o$$

$$F^{23}_{ikm} = \int \eta_i\, \eta_k\, \gamma'_m\, d\bar{x}_o \qquad\qquad L^{20}_{im} = \int \gamma_i\, \gamma'_m\, d\bar{x}_o$$

$$F^{24}_{ikm} = \int \eta_i\, \eta_k\, \gamma'_m\, d\bar{x}_o \qquad\qquad L^{21}_{ikm} = \int \gamma_i\, \eta'_k\, \gamma'_m\, d\bar{x}_o$$

$$L^{22}_{ikm} = \int \gamma_i\, \eta_k\, \gamma'_m\, d\bar{x}_o$$

$$L^{23}_{im} = \int \gamma_i\, \gamma'_m\, \bar{x}\, d\bar{x}_o$$

$$L^{24}_{ik\ell} = \int \gamma_i\, \eta'_k\, \eta'_\ell\, d\bar{x}_o$$

APPENDIX C

GENERALIZED AERODYNAMIC LOADS AND ELEMENTS

OF THE COEFFICIENT MATRIX AND FORCING VECTOR

C.1 Generalized Aerodynamic Loads

In evaluating the generalized aerodynamic loading terms, one encounters a considerable number of terms which are small and therefore negligible. In order to neglect the appropriate terms, a rational ordering scheme is used which enables one to neglect terms in a systematic manner. In this scheme all the important parameters of the problem are assigned orders of magnitude in terms of a typical displacement quantity ε_D thus:

$$\eta_k = 0(1) \qquad g_k = 0(\varepsilon_D) \qquad c_{Do}/a = 0(\varepsilon_D^2)$$

$$\gamma_m = 0(1) \qquad h_m = 0(\varepsilon_D) \qquad \bar{x} = 0(1)$$

$$\eta_k' = 0(1) \qquad \overset{*}{g}_k = 0(\varepsilon_D) \qquad \mu = 0(1)$$

$$\gamma_m' = 0(1) \qquad \overset{*}{h}_m = 0(\varepsilon_D) \qquad \sin\psi = 0(1)$$

$$\beta_P = 0(\varepsilon_D) \qquad \lambda = 0(\varepsilon_D) \qquad \cos\psi = 0(1)$$

$$\beta_D = 0(\varepsilon_D) \qquad \theta = 0(\varepsilon_D)$$

An order of magnitude analysis of the equations indicates that in general terms up to and including $0(\varepsilon_D^2)$ must be included in the linearized flap equation, while for the lag equation some $0(\varepsilon_D^3)$ terms have to be retained. These higher order terms in the aerodynamic part of the flap and lag equations will be marked by a ╱ and neglected.

The aerodynamic loading terms L_z and L_y are given by the expressions:

$$L_z = ab\rho_A R^3\Omega^2\left[\bar{x}^2\theta + 2\bar{x}\mu \sin\psi\theta - 2\bar{x}\mu \cos\psi\ \underline{\gamma_m' h_m \theta}\right.$$

$$\left. - 2\bar{x}\mu\ \cancel{\cos\psi}\ \beta_D\ \theta^2 - 2\bar{x}\frac{\ell}{R}\gamma_m\overset{*}{h}_m\ \theta + \frac{\mu^2}{2}(1-\cos 2\psi)\theta - \mu^2 \sin 2\psi\ \underline{\gamma_m' h_m}\ \theta \right.$$

$$- \mu^2 \sin 2\psi \, \beta_D \, \theta^2 - 2\mu \sin\psi \frac{\ell}{R} \gamma_m \overset{*}{h}_m \, \theta + \frac{\mu^2}{2} (1+\cos 2\psi)\gamma_m' \gamma_r' h_m h_r \, \theta$$

$$+ \mu^2 (1+\cos 2\psi)\gamma_m' h_m \beta_D \theta^2 + 2\mu \cos\psi \, \gamma_m' h_m \frac{\ell}{R} \gamma_r \overset{*}{h}_r \, \theta + \frac{\mu^2}{2}(1+\cos 2\psi)\beta_D^2 \, \theta^3$$

$$+ 2\mu \cos\psi \, \beta_D \, \theta^2 \frac{\ell}{R} \gamma_m \overset{*}{h}_m - \bar{x} \frac{\ell}{R} \eta_k \overset{*}{g}_k - \bar{x}\lambda - \bar{x}\mu \cos\psi(\beta_P + \beta_D)$$

$$- \bar{x}\mu \cos\psi \, \eta_k g_k - \mu \sin\psi \frac{\ell}{R} \eta_k \overset{*}{g}_k - \mu \sin\psi\lambda - \frac{\mu^2}{2}\sin 2\psi(\beta_D + \beta_D)$$

$$- \frac{\mu^2}{2}\sin 2\psi \, \eta_k' g_k + \mu \cos\psi\gamma_m' h_m \frac{\ell}{R}\eta_k \overset{*}{g}_k + \mu \cos\psi \, \gamma_m' h_m \, \lambda$$

$$+ \frac{\mu^2}{2}(1+\cos 2\psi)\gamma_m' h_m(\beta_P+\beta_D) + \frac{\mu^2}{2}(1+\cos 2\psi)\gamma_m' h_m \eta_k' g_k$$

$$+ \mu \cos\psi\beta_D \theta \frac{\ell}{R}\eta_k \overset{*}{g}_k + \mu\cos\psi\beta_D \theta\lambda + \frac{\mu^2}{2}(1+\cos 2\psi)\beta_D\theta(\beta_P+\beta_D)$$

$$+ \frac{\mu^2}{2}(1+\cos 2\psi)\beta_D\theta\eta_k' g_k + \frac{\mu^2}{R^2}\gamma_m \overset{*}{h}_m \eta_k \overset{*}{g}_k + \frac{\ell}{R}\gamma_m \overset{*}{h}_m \lambda + \frac{\ell}{R}\gamma_m \overset{*}{h}_m \mu\cos\psi(\beta_P+\beta_D)$$

$$+ \frac{\ell}{R}\gamma_m \overset{*}{h}_m \mu \cos\psi\eta_k' g_k + \frac{\ell^2}{R^2}\gamma_m \gamma_r \overset{*}{h}_m \overset{*}{h}_r \, \theta \Big] \tag{C.2}$$

$$L_y = -ab\rho_A R^3\Omega^2 \Bigg\{ \theta\Bigg[\frac{\ell}{R}\eta_k \overset{*}{g}_k \, \bar{x} + \frac{\ell}{R}\eta_k g_k \, \mu\sin\psi - \frac{\ell}{R}\eta_k \overset{*}{g}_k \, \mu\cos\psi\gamma_m' hm$$

$$- \frac{\ell}{R}\eta_k \overset{*}{g}_k \beta_D \, \theta - \frac{\ell^2}{R^2}\eta_k \overset{*}{g}_k \gamma_m \overset{*}{h}_m + \lambda\bar{x} + \lambda\mu\sin\psi - \lambda\mu\cos\psi\gamma_m' hm$$

$$- \lambda\mu\cos\psi\beta_D \, \theta - \lambda\frac{\ell}{R}\gamma_m \overset{*}{h}_m + \mu\cos\psi(\beta_P+\beta_D)\bar{x} + \frac{\mu^2}{2}\sin 2\psi(\beta_P+\beta_D)$$

$$- \frac{\mu^2}{2}(1+\cos 2\psi)(\beta_P+\beta_D)\gamma_m' h_m - \frac{\mu^2}{2}(1+\cos 2\psi)(\beta_P+\beta_D)\beta_D \, \theta - \mu\cos\psi(\beta_P+\beta_D)\frac{\ell}{R}\gamma_m \overset{*}{h}_m$$

$$+ \mu\cos\psi\eta_k' g_k \, \bar{x} + \frac{\mu^2}{2}\sin 2\psi\eta_k' g_k - \frac{\mu^2}{2}(1+\cos 2\psi)\eta_k' g_k\gamma_m' h_m$$

$$- \frac{\mu^2}{2}(1+\cos 2\psi)\eta_k' g_k\beta_D \, \theta - \mu\cos\psi\eta_k' g_k \frac{\ell}{R}\gamma_m \overset{*}{h}_m \Bigg] - \frac{\ell^2}{R^2}\eta_k \overset{*}{g}_k \eta_\ell \overset{*}{g}_\ell - 2\lambda\frac{\ell}{R}\eta_k \overset{*}{g}_k$$

$$-2\frac{\ell}{R}\eta_k \overset{*}{g}_k \mu\cos\psi(\beta_P+\beta_D) - \frac{\ell}{R}\eta_k \overset{*}{g}_k \mu\cos\psi\eta_\ell g_\ell - \lambda^2 - 2\lambda\mu\cos\psi(\beta_P+\beta_D)$$

68

$$- 2\lambda\mu \cos\psi \; \eta_k' \; g_k - \frac{\mu^2}{2} (1+\cos 2\psi)(\beta_P+\beta_D)^2 - \mu^2(1+\cos 2\psi)(\beta_P+\beta_D)\eta_k' \; g_k$$

$$- \frac{\mu^2}{2} (1+\cos 2\psi)\eta_k' \; g_k \; \eta_\ell' \; g_\ell + \frac{C_{Do}}{a}\left[\bar{x}^2 + 2\bar{x} \; \mu \sin\psi - 2\bar{x}\mu \; \cos\psi \; \gamma_m' \; h_m \right.$$

$$- 2\bar{x}\mu \; \cos\psi \; \beta_D \; \theta - 2\bar{x} \; \frac{\ell}{R} \; \gamma_m \; \overset{*}{h}_m + \frac{\mu^2}{2} (1-\cos 2\psi) - \mu^2 \sin 2\psi \; \gamma_m' \; h_m$$

$$- \mu^2 \sin 2\psi \; \beta_D \; \theta - 2\mu \; \sin\psi \; \frac{\ell}{R} \; \gamma_m \; \overset{*}{h}_m + \frac{\mu^2}{2} (1+\cos 2\psi)\gamma_m' \; h_m \; \gamma_r' \; h_r$$

$$+ \mu^2(1+\cos 2\psi)\gamma_m' h_m \; \beta_D \; \theta + 2\mu \; \cos\psi \; \gamma_m' \; h_m \; \gamma_r \; \overset{*}{h}_r + \frac{\mu^2}{2} (1+\cos 2\psi)\beta_D^2 \; \theta^2$$

$$\left.\left.+ 2\mu \; \cos\psi \; \beta_D \; \theta \; \frac{\ell}{R} \; \gamma_m \; \overset{*}{h}_m + \frac{\ell^2}{R^2} \; \gamma_m \; \overset{*}{h}_m \; \gamma_r \; \overset{*}{h}_r \right]\right\} \tag{C.3}$$

Where the terms in the lag equation underlined by _____ are $0(\epsilon_D^3)$. Also, terms in both equations associated with radial flow are underscored with

— — — — — — — —.

Using these equations and the definition of the flap and lag coefficients given in Appendix B, the generalized aerodynamic forces are

$$A_{Fi} = \frac{\ell^2}{\Omega I_b} \int_{\underline{A}}^{\bar{B}} L_z \eta_i d\bar{x}_o = \frac{\gamma}{2} \left(\frac{\ell}{R}\right)^2 \left\{ F_i^1 \; \theta + F_i^2 \; 2\mu \; \theta \; \sin\psi \right.$$

$$- F_i^2 \; \mu \; \cos\psi(\beta_P+\beta_D) + F_i^3 \; \frac{\mu^2}{2} \; \theta(1-\cos 2\psi) - F_i^3 \; \frac{\mu^2}{2} \; \sin 2\psi(\beta_P+\beta_D)$$

$$- F_i^2 \; \lambda - F_i^3 \; \lambda\mu \; \sin\psi + \left[- F_{ik}^6 \; \mu \; \cos\psi - F_{ik}^7 \; \frac{\mu^2}{2} \; \sin 2\psi\right] g_k$$

$$+ \left[- F_{ik}^8 \; \frac{\ell}{R} - F_{ik}^9 \; \mu \; \frac{\ell}{R} \; \sin\psi\right] \overset{*}{g}_k + \left[- F_{im}^{21} \; 2\mu \; \cos\psi\theta + F_{im}^{22} \; \mu\lambda \; \cos\psi \right.$$

$$\left.- F_{im}^{22} \; \mu^2 \; \theta \; \sin 2\psi + F_{im}^{22} \; \frac{\mu^2}{2} \; (\beta_P+\beta_D) \; (1+\cos 2\psi)\right] h_m + \left[- F_{im}^{10} \; 2 \; \frac{\ell}{R} \; \theta\right.$$

$$\left.- F_{im}^{11} \; \mu \; \frac{\ell}{R} \; 2 \; \sin\psi\theta + F_{im}^{11} \; \mu \; \frac{\ell}{R} \; \cos\psi(\beta_P+\beta_D) + F_{im}^{11} \; \lambda \; \frac{\ell}{R}\right] \overset{*}{h}_m$$

$$+ F_{ikm}^{23} \; \frac{\mu^2}{2} \; (1+\cos 2\psi)g_k h_m + F_{ikm}^{14} \; \frac{\ell}{R} \; \mu \; \cos\psi \; g_k \overset{*}{h}_m$$

$$\left.+ F_{ikm}^{24} \; \mu \; \cos\psi \; \frac{\ell}{R} \; \overset{*}{g}_k \; h_m + F_{ikm}^{15} \; \left(\frac{\ell}{R}\right)^2 \; \overset{*}{g}_k \; \overset{*}{h}_m \right\} \tag{C.4}$$

$$A_{Li} = -\frac{\ell^2}{\Omega I_b} \int_A^{\bar{B}} L_y \, \gamma_i \, d\bar{x}_o = \frac{\gamma}{2}\left(\frac{\ell}{R}\right)^2 \left\{ L_i^1 \, \lambda\theta + L_i^1 \, \mu(\beta_P+\beta_D)\cos\psi\theta \right.$$

$$+ L_i^1 \, 2\mu \, \frac{C_{Do}}{a} \sin\psi - L_i^2 \, \lambda^2 - L_i^2 \, \frac{\mu^2}{2} (1+\cos 2\psi)(\beta_P+\beta_D)^2 + L_i^2 \, \frac{\mu^2}{2} \, \frac{C_{Do}}{a} (1-\cos 2\psi)$$

$$- L_i^2 \, \lambda \, 2\mu(\beta_P+\beta_D)\cos\psi + L_i^2 \, \lambda\mu\theta \, \sin\psi + L_i^2 \, \frac{\mu^2}{2} (\beta_P+\beta_D)\theta \, \sin 2\psi$$

$$+ L_i^4 \, \frac{C_{Do}}{a} + \left[L_{ik}^{10} \, \mu \, \cos\psi\theta + L_{ik}^{11} \, \frac{\mu^2}{2} \sin 2\psi\theta - L_{ik}^{11} \, \mu^2(\beta_P+\beta_D)(1+\cos 2\psi) \right.$$

$$\left. - L_{ik}^{11} \, 2\lambda\mu \, \cos\psi \right] g_k + \left[L_{ik}^7 \, \frac{\ell}{R} \, \theta + L_{ik}^8 \, \frac{\ell}{R} \, \mu \, \sin\psi\theta - L_{ik}^8 \, 2\mu \, \frac{\ell}{R} \cos\psi(\beta_P+\beta_D) \right.$$

$$\left. - L_{ik}^8 \, 2\lambda \, \frac{\ell}{R} \right] \overset{*}{g}_k + \left[L_{im}^{20} \, \lambda\mu \, \cos\psi\theta - L_{im}^{20} \, \frac{\mu^2}{2} (\beta_P+\beta_D)\theta(1+\cos 2\psi) \right.$$

$$- L_{im}^{20} \, \mu^2 \, \frac{C_{Do}}{a} \sin 2\psi - L_{im}^{23} \, 2\mu \, \cos\psi \, \frac{C_{Do}}{a} \right] h_m + \left[- L_{im}^{13} \, \mu \, \cos\psi(\beta_P+\beta_D) \, \frac{\ell}{R} \, \theta \right.$$

$$\left. - L_{im}^{13} \, 2\mu \, \sin\psi \, \frac{\ell}{R} \, \frac{C_{Do}}{a} - L_{im}^{14} \, 2 \, \frac{\ell}{R} \, \frac{C_{Do}}{a} - L_{im}^{13} \, \lambda \, \frac{\ell}{R} \, \theta \right] \overset{*}{h}_m$$

$$- L_{ik\ell}^{24} \, \frac{\mu^2}{2} (1+\cos 2\psi) \, g_k g_\ell - L_{ikm}^{21} \, \frac{\mu^2}{2} (1+\cos 2\psi)\theta g_k h_m - L_{ik\ell}^7 \, 2 \, \frac{\ell}{R} \, \mu \, \cos\psi \, \overset{*}{g}_k g_\ell$$

$$- L_{ikm}^{16} \, \mu \, \cos\psi \, \frac{\ell}{R} \, \theta \, g_k \overset{*}{h}_m - L_{ikm}^{22} \, \frac{\ell}{R} \, \mu \, \cos\psi\theta \, \overset{*}{g}_k h_m - L_{ik\ell}^{18} \left(\frac{\ell}{R}\right)^2 \overset{*}{g}_k \overset{*}{g}_\ell$$

$$\left. - L_{ikm}^{19} \left(\frac{\ell}{R}\right)^2 \theta \, \overset{*}{g}_k \overset{*}{h}_m \right\} \tag{C.5}$$

C.2   Elements of the $\underset{\sim}{A}$ Matrix

The elements of the $\underset{\sim}{A}$ matrix, which defines the equations of motion when written as first order differential equations, are given below

$$A_{21} = 1; \quad A_{22} = A_{23} = A_{24} = 0$$

$$A_{43} = 1; \quad A_{41} = A_{42} = A_{44} = 0$$

$$A_{11} = -2\eta_{SF1}\,\overline{\omega}_{F1} + \frac{1}{\overline{M}_{F1}}\left\{\frac{\gamma}{2}\left(\frac{\ell}{R}\right)^2\left[-F^8\,\frac{\ell}{R} - F^9\,\mu\,\frac{\ell}{R}\sin\psi + F^{24}\,\mu\,\cos\psi\,\frac{\ell}{R}\,h_1^o\right]\right\}$$

$$A_{12} = -\overline{\omega}_{F1}^2 + \frac{1}{\overline{M}_{F1}}\left\{-\overline{E^s} + \frac{\gamma}{2}\left(\frac{\ell}{R}\right)^2\left[-F^6\,\mu\,\cos\psi - F^7\,\frac{\mu^2}{2}\sin 2\psi\right.\right.$$

$$\left.\left. + F^{23}\,\frac{\mu^2}{2}(1+\cos 2\psi)h_1^o\right]\right\}$$

$$A_{13} = \frac{1}{\overline{M}_{F1}}\left\{2\overline{P}_{111}\,g_1^o + 2(\beta_P+\beta_D)\overline{B^3_{11}} + \frac{\gamma}{2}\left(\frac{\ell}{R}\right)^2\left[-F^{10}\,2\,\frac{\ell}{R}\,\theta - F^{11}\,\mu\,\frac{\ell}{R}\,2\theta\,\sin\psi\right.\right.$$

$$\left.\left. + F^{11}\,\frac{\ell}{R}\cos\psi\mu(\beta_P+\beta_D) + F^{11}\lambda\,\frac{\ell}{R} + F^{14}\,\frac{\ell}{R}\,\mu\,\cos\psi\,g_1^o\right]\right\}$$

$$A_{14} = \frac{1}{\overline{M}_{F1}}\left\{\overline{E^{cs}} + \frac{\gamma}{2}\left(\frac{\ell}{R}\right)^2\left[-F^{21}2\mu\theta\,\cos\psi + F^{22}\mu\lambda\,\cos\psi - F^{22}\,\mu^2\,\theta\,\sin 2\psi\right.\right.$$

$$\left.\left. + F^{22}\,\frac{\mu^2}{2}(\beta_P+\beta_D)(1+\cos 2\psi) + F^{23}\,\frac{\mu^2}{2}(1+\cos 2\psi)g_1^o\right]\right\}$$

$$A_{31} = \frac{1}{\overline{M}_{F1}}\left\{-2\overline{M}_{\eta_{111}}g_1^o - 2(\beta_P+\beta_D)\overline{B^7_{11}} + \frac{\gamma}{2}\left(\frac{\ell}{R}\right)^2\left[L^7\,\frac{\ell}{R}\,\theta + L^8\,\frac{\ell}{R}\,\mu\theta\,\sin\psi\right.\right.$$

$$\left.\left. - L^8\,2\mu\,\frac{\ell}{R}\cos\psi(\beta_P+\beta_D) - L^8 2\lambda\,\frac{\ell}{R} - L^{17}2\,\frac{\ell}{R}\,\mu\,\cos\psi\,g_1^o - L^{22}\,\frac{\ell}{R}\,\mu\,\cos\psi\theta\,h_1^o\right]\right\}$$

$$A_{32} = \frac{1}{\overline{M}_{L1}}\left\{\overline{\overline{E^{cs}}} + \frac{\gamma}{2}\left(\frac{\ell}{R}\right)^2\left[L^{10}\,\mu\,\cos\psi\theta + L^{11}\,\frac{\mu^2}{2}\,\theta\,\sin 2\psi\right.\right.$$

$$\left.\left. - L^{11}\,\mu^2(\beta_P+\beta_D)(1+\cos 2\psi) - L^{11}2\lambda\mu\,\cos\psi - L^{24}\,\mu^2(1+\cos 2\psi)\,g_1^o\right.\right.$$

$$\left.\left. - L^{21}\,\frac{\mu^2}{2}(1+\cos 2\psi)\theta h_1^o\right]\right\}$$

$$A_{33} = -2\eta_{SL1}\,\overline{\omega}_{L1} + \frac{1}{\overline{M}_{L1}}\left\{h_1^o\left(2\overline{S}_{111} - 2\overline{M}_{\gamma_{111}}\right) + 2\,\beta_D\theta\,\overline{B^8_{11}}\right.$$

$$\left. + \frac{\gamma}{2}\left(\frac{\ell}{R}\right)^2\left[-L^{13}\,\mu\,\cos\psi(\beta_P+\beta_D)\,\frac{\ell}{R}\,\theta - L^{13}\,2\mu\,\sin\psi\,\frac{\ell}{R}\,\frac{C_{Do}}{a} - L^{14}\,2\,\frac{\ell}{R}\,\frac{C_{Do}}{a}\right.\right.$$

$$\left.\left. - L^{13}\,\lambda\,\frac{\ell}{R}\,\theta - L^{16}\,\mu\,\cos\psi\,\frac{\ell}{R}\,\theta\,g_1^o\right]\right\}$$

$$A_{34} = - \overline{\omega}_{L1}^2 + \frac{1}{\overline{M}_{L1}} \left\{ \overline{\overline{E^s}} + \frac{\gamma}{2} \left(\frac{\ell}{R}\right)^2 \left[- L^{20} \lambda\mu \cos\psi\theta - L^{20} \frac{\mu^2}{2} (\beta_P + \beta_D)\theta(1 + \cos 2\psi) \right.\right.$$

$$\left.\left. - L^{20} \mu^2 \frac{C_{Do}}{a} \sin 2\psi - L^{23} 2\mu \cos\psi \frac{C_{Do}}{a} - L^{21} \frac{\mu^2}{2} (1 + \cos 2\psi)\theta g_1^o \right] \right\}$$

C.3 Elements of the f Vector

The elements of the f vector, which defines the forcing terms when the equations of motion are written as first order differential equations, are given below

$$f_2 = f_4 = 0$$

$$f_1 = \frac{1}{\overline{M}_{F1}} \frac{\gamma}{2} \left(\frac{\ell}{R}\right)^2 \left\{ F^2 \mu \left[2\theta \sin\psi - \cos\psi(\beta_P + \beta_D) \right] + F^3 \mu^2 \left[\frac{\theta}{2}(1 - \cos 2\psi) \right.\right.$$

$$\left. - \frac{1}{2} \sin 2\psi(\beta_P + \beta_D) \right] - F^3 \lambda\mu \sin\psi + \left[- F^6 \mu \cos\psi - F^7 \frac{\mu^2}{2} \sin 2\psi \right] g_1^o$$

$$+ \left[- F^{21} 2\mu\theta \cos\psi - F^{22} \mu\lambda \cos\psi + F^{22} \mu^2\theta \sin 2\psi \right.$$

$$\left.\left. - F^{22} \frac{\mu^2}{2} (\beta_P + \beta_D)(1 + \cos 2\psi) \right] h_1^o + \left[F^{23} \frac{\mu^2}{2} (1 + \cos 2\psi) \right] g_1^o h_1^o \right\}$$

$$f_3 = \frac{1}{\overline{M}_{L1}} \frac{\gamma}{2} \left(\frac{\ell}{R}\right)^2 \left\{ - L^2 \frac{\mu^2}{2} (\beta_P + \beta_D)^2 (1 + \cos 2\psi) + L^2 \frac{\mu^2}{2} \frac{C_{Do}}{a} (1 + \cos 2\psi) + \right.$$

$$+ \left[L^1 \mu(\beta_P + \beta_D)\theta - L^2 \lambda 2\mu(\beta_P + \beta_D) \right] \cos\psi + \left[L^1 2\mu \frac{C_{Do}}{a} + L^2 \lambda\mu\theta \right] \sin\psi$$

$$+ \left[L^2 \frac{\mu^2}{2} (\beta_P + \beta_D)\theta \right] \sin 2\psi + \left[L^{10} \mu \cos\psi\theta + L^{11} \frac{\mu^2}{2} \theta \sin 2\psi \right.$$

$$\left. - L^{11} \mu^2 (\beta_P + \beta_D)(1 + \cos 2\psi) - L^{11} 2\lambda\mu \cos\psi \right]$$

$$+ \left[- L^{20} \lambda\mu\theta \cos\psi - L^{20} \frac{\mu^2}{2} (\beta_P + \beta_D)\theta(1 + \cos 2\psi) - L^{20} \mu^2 \frac{C_{Do}}{a} \sin 2\psi \right.$$

$$\left. - L^{23} 2\mu \cos\psi \frac{C_{Do}}{a} \right] h_1^o + \left[- L^{24} \frac{\mu^2}{2} (1 + \cos 2\psi) \right] g_1^{o^2} + \left[- L^{21} \frac{\mu^2}{2} (1 + \cos 2\psi)\theta \right] g_1^o h_1^o \right\}$$

APPENDIX D

REGION OF REVERSED FLOW

The circular region of reversed flow, which exists over the retreating blade, is quite well known. In past treatments of reversed flow it has been customary (Ref. 3) to define three separate regions: (a) normal flow, (b) (b) reversed flow, (c) mixed flow, and evaluate the appropriate aerodynamic expressions for each region. When this model is used together with a modal representation of the blade, the evaluation of the generalized aerodynamic expressions F_i, L_i becomes quite cumbersome, and a more convenient procedure had to be devised.

The approximate reversed flow model developed for the present study consists of replacing the circular region by an approximate region which has two straight boundaries and a circular one as shown in Fig. 2. The approximation is based on the assumption that the area contained in the circular region must be equal to the area contained in the approximate region. Two separate cases must be considered: (1) $\mu < 1$, (2) $\mu \geq 1$.

Case (1). For $\mu < 1$, the diameter of the circular sector is taken as μ. Simple geometric considerations show that the angle α is always a constant given by

$$\alpha = \pi/2 \tag{D.1}$$

Case (2). For $\mu \geq 1$, simple geometric considerations show that

$$\alpha = \pi - 2 \sin^{-1}\left(\frac{1}{\mu}\right) + \mu^2 \sin^{-1}\left(\frac{1}{\mu}\right) - \sqrt{\mu^2 - 1} \tag{D.2}$$

Thus for $\mu < 1$ the generalized aerodynamic loads in the mixed flow region are calculated from

$$\overline{A}_{Fi} = \frac{\ell^2}{\Omega^2 I_b}\left[-\int_{\underline{A}}^{\mu} L_z \, \eta_i \, d\bar{x}_o + \int_{\mu}^{\overline{B}} L_z \, \eta_i \, d\bar{x}_o\right] \tag{D.3}$$

73

$$\bar{A}_{Li} = -\frac{\ell^2}{\Omega^2 I_b} \left[-\int_{\bar{A}}^{\mu} L_y \gamma_i \, d\bar{x}_o + \int_{\mu}^{\bar{B}} L_y \gamma_i \, d\bar{x}_o \right] \tag{D.4}$$

while for $\mu \geq 1.0$

$$\bar{A}_{Fi} = \frac{\ell^2}{\Omega^2 I_b} \left[-\int_{\bar{A}}^{\bar{B}} L_z \eta_i \, d\bar{x}_o \right] = -A_{Fi} \tag{D.5}$$

$$\bar{A}_{Li} = -\frac{\ell^2}{\Omega^2 I_b} \left[-\int_{\bar{A}}^{\bar{B}} L_y \gamma_i \, d\bar{x}_o \right] = -A_{Li} \tag{D.6}$$

These equations are based on the assumption that the lift curve slope in the reversed flow region is equal to the negative value of the lift curve slope in normal flow.

74

APPENDIX E

ELASTIC COUPLING

The angle of collective pitch θ is the source of the so called elastic coupling effect in cantilevered rotor blades. This effect couples the bending perpendicular to the hub plane with the bending parallel to the hub plane. For convenient representation of this effect, the elastic coupling terms in Eq. (2.1) must be rewritten

$$(EI)_y \cos^2\theta + (EI)_z \sin^2\theta = (EI)_y + \left[(EI)_z-(EI)_y\right]\sin^2\theta \tag{E.1}$$

$$(EI)_y \sin^2\theta + (EI)_z \cos^2\theta = (EI)_z - \left[(EI)_z-(EI)_y\right]\sin^2\theta \tag{E.2}$$

Defining

$$E_{c1} = \left[(EI)_z-(EI)_y\right]\sin^2\theta \tag{E.3}$$

$$E_{c2} = \left[(EI)_z-(EI)_y\right]\sin\theta\cos\theta \tag{E.4}$$

When applying Galerkin's method on the equations of motion, it is convenient to define the following additional expressions

$$\overline{E^s_{ik}} = \frac{\dfrac{1}{\ell}\displaystyle\int_o^1 E_{c1}\,\eta''_i\,\eta''_k\,d\bar{x}_o}{\Omega^2 I_b} \tag{E.5}$$

$$\overline{E^{cs}_{im}} = \frac{\dfrac{1}{\ell}\displaystyle\int_o^1 E_{c2}\,\eta''_i\,\gamma''_m\,d\bar{x}_o}{\Omega^2 I_b} \tag{E.6}$$

$$\overline{\overline{E^s_{im}}} = \frac{\dfrac{1}{\ell}\displaystyle\int_o^1 E_{c1}\,\gamma''_i\,\gamma''_m\,d\bar{x}_o}{\Omega^2 I_b} \tag{E.7}$$

$$\overline{\overline{E^{cs}_{ik}}} = \frac{\dfrac{1}{\ell}\displaystyle\int_o^1 E_{c2}\,\gamma''_i\,\eta''_k\,d\bar{x}_o}{\Omega^2 I_b} \tag{E.8}$$

75